

Article

Estimating Ground-Level Particulate Matter in Five Regions of China Using Aerosol Optical Depth

Qiaolin Zeng ^{1,2,3}, **Jinhua Tao** ^{2,*}, **Liangfu Chen** ^{2,4}, **Hao Zhu** ³, **SongYan Zhu** ⁵ and **Yang Wang** ⁶¹ The College of Computer Science and Technology, Chongqing University of Posts and Telecommunications, Chongqing 400065; China; zengql@cqupt.edu.cn² State Key Laboratory of Remote Sensing Science, Aerospace Information Research Institute, Chinese Academy of Sciences, Beijing Normal University, Beijing 100101, China; Chenlf@radi.ac.cn³ Chongqing Institute of Meteorological Sciences, Chongqing 401147, China; zengql@radi.ac.cn⁴ University of Chinese Academy of Sciences, Beijing 100049, China⁵ The Department of Geography, University of Exeter, Rennes Drive, Exeter EX4 4RJ, UK; sz394@exeter.ac.uk⁶ School of Geography, Fujian Normal University, Fujian 350007, China; Wangyang@fjnu.edu.cn

* Correspondence: taojh@radi.ac.cn

Received: 1 February 2020; Accepted: 5 March 2020; Published: 9 March 2020



Abstract: Aerosol optical depth (AOD) has been widely used to estimate near-surface particulate matter (PM). In this study, ground-measured data from the Campaign on Atmospheric Aerosol Research network of China (CARE-China) and the Aerosol Robotic Network (AERONET) were used to evaluate the accuracy of Visible Infrared Imaging Radiometer Suite (VIIRS) AOD data for different aerosol types. These four aerosol types were from dust, smoke, urban, and uncertain and a fifth “type” was included for unclassified (i.e., total) aerosols. The correlation for dust aerosol was the worst ($R^2 = 0.15$), whereas the correlations for smoke and urban types were better (R^2 values of 0.69 and 0.55, respectively). The mixed-effects model was used to estimate the $PM_{2.5}$ concentrations in Beijing–Tianjin–Hebei (BTH), Sichuan–Chongqing (SC), the Pearl River Delta (PRD), the Yangtze River Delta (YRD), and the Middle Yangtze River (MYR) using the classified aerosol type and unclassified aerosol type methods. The results suggest that the cross validation (CV) of different aerosol types has higher correlation coefficients than that of the unclassified aerosol type. For example, the R^2 values for dust, smoke, urban, uncertain, and unclassified aerosol types BTH were 0.76, 0.85, 0.82, 0.82, and 0.78, respectively. Compared with the daily $PM_{2.5}$ concentrations, the air quality levels estimated using the classified aerosol type method were consistent with ground-measured $PM_{2.5}$, and the relative error was low (most RE was within $\pm 20\%$). The classified aerosol type method improved the accuracy of the $PM_{2.5}$ estimation compared to the unclassified method, although there was an overestimation or underestimation in some regions. The seasonal distribution of $PM_{2.5}$ was analyzed and the $PM_{2.5}$ concentrations were high during winter, low during summer, and moderate during spring and autumn. Spatially, the higher $PM_{2.5}$ concentrations were predominantly distributed in areas of human activity and industrial areas.

Keywords: VIIRS AOD; $PM_{2.5}$; aerosol type; mixed-effects model; China

1. Introduction

Studies have shown that human health can be affected by long-term exposure to fine particulate matter (PM, with a diameter of $< 2.5 \mu m$), and $PM_{2.5}$ is associated with various diseases such as respiratory tract infections and lung diseases [1–4]. With rapid economic development, urbanization, and industrialization, China has become one of the most polluted regions in the world [5,6]. Since 2013, the China National Environmental Monitoring Center (CNEMC) has established numerous

ground-measured PM_{2.5} observation stations that are significant to the assessment of air quality in China. The accuracy of ground-measured observations is high, but this method has certain limitations in terms of spatial coverage, and the diversity of pollutant sources hinders the assessment of complex air quality models [7–9]. In contrast, satellite remote sensing technology can compensate by providing high spatial resolution over large regions.

The columnar integrated aerosol optical depth (AOD) represents the extinction of incoming solar radiation by aerosols and its magnitude is directly proportional to the loading of aerosols in the total atmospheric column [10–12]. A series of satellites have carried sensors capable of retrieving AOD, which are widely used to estimate near-surface PM_{2.5} concentrations; these satellites include the Moderate Resolution Imaging Spectroradiometer (MODIS) [13–17], the Multiangle Imaging Spectroradiometer (MISR) [2,18–20], the Visible Infrared Imaging Radiometer Suite (VIIRS) [13,18,21–23], and Himawari-8 [24], et al. The commonly used methods for estimating PM_{2.5} concentrations from AOD are the proportional factor method [25,26], the semiempirical formula method [16,27,28], and the statistical model method [7,13,19,24,29]. The proportional factor method and the statistical model method are widely used by researchers to estimate regional PM_{2.5} concentrations based on the relationship between AOD and PM_{2.5}; however, the influence of the aerosol compositions on the estimation results has not been considered. The semiempirical formula method is based on the physical mechanism of the relationship between parameters such as the vertical profile and particle size. The PM_{2.5} compositions vary with different regions, and the method for unconsidered aerosol types is thus difficult to use in a large region with few ground-measurement stations. Therefore, Sunkun et al. proposed a local aerosol concept to distinguish anthropogenic and natural source aerosols using MODIS AOD to estimate PM_{2.5} in different regions and seasons [30]. The results showed that the correlations had large differences over both seasons and regions. Chen et al. collected AErosol RObotic NETwork (AERONET) data from the Xuzhou and Beijing sites and classified aerosols into urban type, continental type, dust type, and biomass burning type [31]. The correlation coefficient between AOD and PM_{2.5} increased from 0.25 to 0.34, and the classified aerosol type method thus improved the PM_{2.5} estimation accuracy. Additionally, the results showed that the urban and biomass burning aerosol types had the best accuracy, and that the dust aerosol type was the worst. However, observation stations have limitations due to various unfavorable conditions (such as terrain and climate), which makes the method proposed by Sunkun difficult to generalize to large-scale regions. Previous studies have shown that the classified aerosol type method can improve the PM_{2.5} estimation accuracy as long as the ground station is nearby. Therefore, the classified aerosol type method is not widely used for satellite data due to a lack of aerosol type information. However, since 2012, the VIIRS AOD product has provided aerosol type attributes, which offers the possibility of PM_{2.5} estimation from satellite data using this method.

Many studies ([27,32–34]) have shown that the most polluted areas in China are mainly located in Beijing–Tianjin–Hebei (BTH), Sichuan–Chongqing (SC), the Pearl River Delta (PRD), the Yangtze River Delta (YRD), and the Middle Yangtze River (MYR); the locations of these areas are shown in Figure 1. For this paper, we obtained VIIRS AOD to estimate PM_{2.5} concentrations using both classified and unclassified aerosol type methods across typical contaminated areas in China. The ground-measured AOD was obtained to evaluate the accuracy of VIIRS AOD. Then, statistical models were used to estimate PM_{2.5} concentrations using the two methods (classified and unclassified), and the accuracy of the results was verified. The spatiotemporal distribution of PM_{2.5} concentrations in five typical areas were analyzed.

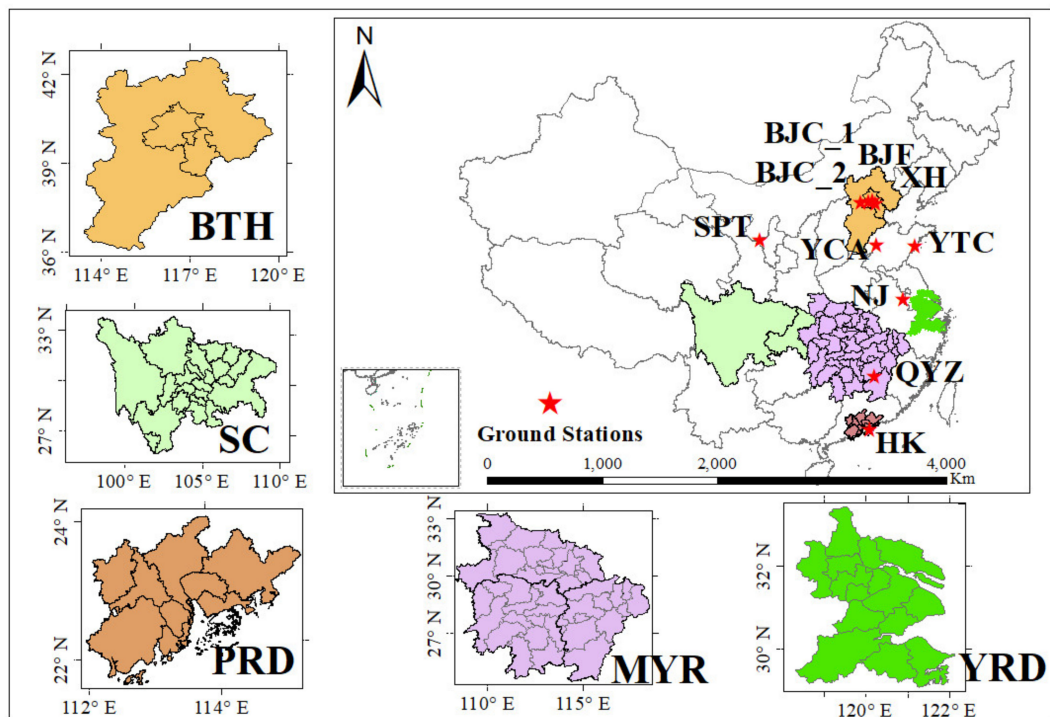


Figure 1. The locations of the five regions in China: Beijing–Tianjin–Hebei (BTH), Sichuan–Chongqing (SC), Pearl River Delta (PRD), Yangtze River Delta (YRD), and Middle Yangtze River (MYR), and the location of the ground_measured aerosol optical depth (AOD).

2. Materials and Methods

2.1. Data

2.1.1. Ground-Measured Aerosol Optical Depth (AOD)

Ground-measured AOD were obtained from the Campaign on Atmospheric Aerosol Research network of China (CARE-China). CARE uses a new generation of portable solar photometers that are produced by the United States (US) Department of Forestry and consist of four channels with center wavelengths of 405, 500, 650, and 880 nm [35]. The measurement periods at each station were set within the transit period of the satellite. Due to confidentiality, only seven data stations could be obtained to evaluate the accuracy of VIIRS AOD. Figure 1 and Table 1 report the geographic distribution and details of the network stations: Shapotou (SPT), Beijing Forest (BJF), Beijing City_1 (BJC_1), Nanjing (NJ), Yucheng Agriculture (YCA), Yantai Coast (YTC), and Qianyanzhou (QYZ). Moreover, considering the uniformity of the station distribution and to verify the accuracy of VIIRS AOD over different surface types, we used three AERONET observations (listed in Table 1, Beijing City_2 (BJC_2), Xianghe (XH), Hong Kong (HK)). AERONET observations can provide the basic characteristics of aerosol optical properties including AOD, Ångström exponent (α), volume size distribution, and so on [36]. There are three levels of AERONET data. The Level 1.0 data are the original data, while the Level 1.5 data are cloud screened, and Level 2.0 data are cloud screened and quality assured. The Level 1.5 and 2.0 products (version 3.0) were used in this study. Cloudy conditions were removed from the dataset. CARE and AERONET AOD at $0.55\text{ }\mu\text{m}$ were calculated by interpolating AOD using the reported angstrom exponents for respective wavelengths to match the VIIRS wavelength and were averaged to within ± 30 minutes of the VIIRS overpass time. VIIRS AOD values were averaged within a 6 km radius of each ground-measurement station.

Table 1. Information about the ground-measurement stations.

No.	Station	Lon (° E)	Lat (° N)	Time	Station type	Source
1	Shapou (SPT)	104.95	37.45	2013. Jan–Dec	Desert background	CARE
2	Beijing Forest (BJF)	115.43	39.97	2013. Jan–Dec	North China background	CARE
3	Beijing City_1 (BJC_1)	116.28	39.98	2013. Jan–Dec, 2016. Jun–Dec	Megacity	CARE
4	Beijing City_2 (BJC_2)	116.38	39.98	2015. Jan–2016. Dec	Megacity	AERONET
5	Xianghe (XH)	116.96	39.75	2015. Jan–2016. Dec	City suburb	AERONET
6	Nanjing (NJ)	118.42	32.12	2016. Jun–Dec	Central city	CARE
7	Yucheng Agriculture (YCA)	116.57	36.85	2013. Jan–Dec	North China country	CARE
8	Yantai Coast (YTC)	120.27	36.05	2013. Jan–Dec	East China sea coast	CARE
9	Qianyanzhou (QYZ)	115.03	26.45	2016. Jun–Dec	South China country	CARE
10	Hong Kong (HK)	114.18	22.30	2015. Jan–2016. Dec	South China sea coast	AERONET

* Note: The data only validated the retrieval VIIRS AOD accuracy.

2.1.2. Visible Infrared Imaging Radiometer Suite AOD

VIIRS was launched aboard the Suomi NPP satellite on October 28, 2011 and is mainly used for global observations of land, sea, and atmospheric parameters. The VIIRS sensor is a 22-band cross-track scanning radiometer with wavelengths that span a range from 0.412 to 12.013 μm . VIIRS has a swath width of 3040 km and a high nominal spatial resolution of 375 m in the five imagery bands, and 750 m in the 16 moderate-resolution bands and the day–night band (DNB). The VIIRS teams provide two types of AOD products, the intermediate product (IP) AOD and the Environmental Data Record (EDR) AOD, with spatial resolutions of 750 m and 6 km, respectively. VIIRS AOD delivers corresponding quality flag (QF) data. QF was set to 0, 1, 2, or 3, which indicate no data and low-, medium-, and high-quality products, respectively. Yao et al. found that including medium-quality VIIRS AOD data increased the spatiotemporal coverage during winter, but leads to a decline in the model accuracy [13]. To minimize the influence of the AOD accuracy, we only used high quality AOD data with QF = 3. We obtained the “model” flag to distinguish the aerosol type. The numbers of 0, 1, 2, 3, and 4 represent dust, smoke-high absorption, smoke-low absorption, urban-clean, and urban-polluted, respectively. The AOD data were freely downloaded from the comprehensive larger array-data stewardship system [37].

2.1.3. PM_{2.5} Data

Ground-based PM_{2.5} data at a temporal resolution of one hour from January 2015 to December 2016 were obtained from the China National Environmental Monitoring Center (CNEMC). PM_{2.5} concentrations are measured using the tapered element oscillating microbalance (TEOM) approach or the beta-attenuation approach, both of which comply with the National Standard for Environmental Air Quality (GB3095-2012) [38]. By screening out outliers, only reliable observations were retained, and the model is thus well formulated and can be reasonably applied to other areas and days. Several preliminary steps were applied to PM_{2.5}: (1) We omitted records with conflicting AOD and PM_{2.5} values (AOD < 50th percentile and PM_{2.5} > 95th percentile, or PM_{2.5} < 50th percentile and AOD > 95th percentile); (2) records with a Pearson correlation coefficient between PM_{2.5} and AOD < 0.1 in one day were removed; (3) data during precipitation were removed because high ambient humidity following precipitation usually results in PM_{2.5} concentrations that cannot be determined reliably; and (4) the average PM_{2.5} of one hour before and after the satellite overpass time was calculated as the input for further analysis.

2.1.4. Auxiliary Data

Meteorological conditions alter ground-level PM_{2.5} concentrations and need to be included when assessing modeling performance [20,39–41]. For example, the planetary boundary layer height (PBLH) is negatively correlated with PM_{2.5} [42]; the relative humidity (RH) and temperature (TM) correlate to particle compositions, wind speed (WS), and wind direction (WD); and can affect the emission and horizontal transport of air pollutants, and the surface pressure (SP) can influence the atmospheric stability and vertical dispersion of air pollution. RH, TMP, WS, WD, and SP were retrieved from the China Meteorological Data Sharing Service System (CMDSSS) for a total of 2380 stations; the data at 14:00 were selected to match the satellite overpass time. PBLH data provided by the ERA-Interim reanalysis were downloaded from the European Center for Medium-Range Weather Forecasts [43]; the spatial resolution was 0.125° × 0.125°, and the temporal resolution was six hours. All the meteorological data selected were the nearest to the satellite overpass time. The elevation data of the study area were obtained from the Shuttle Radar Topographic Mission (SRTM) [44] and have a spatial resolution of approximately 90 m. Population density at 1-km resolution for 2010 was downloaded from the Data Center for Resource and Environmental Sciences, Chinese Academy of Sciences. Since the original projections and spatial resolutions of the datasets varied greatly, all the datasets were reprojected to the WGS-84 coordinate system and were resampled to 6 km × 6 km with ARCGIS, and all independent variables were matched to the PM_{2.5} stations using the nearest sampling site.

2.2. Model and Validation

All datasets were acquired after all data were integrated, and each record corresponds to a specific day and specific site; however, the data changed with the day and site. Data for days with less than four records were removed to build the model. The mixed-effects model is a generalization of the simple linear model. Lee et al. used the mixed-effects model to evaluate the relationship between PM_{2.5} and AOD, and the results reflected the time difference [17]. Subsequently, Tian et al. proposed a semiempirical model to characterize the nonlinearity relationship between AOD and PM_{2.5} [8]. Song et al. employed a general linear model and a semiempirical model to compare the relationship between AOD and PM_{2.5} in the PRD [45]. The accuracy of the regression model can be improved through the integration of the semiempirical model into the line mixed effect model [46]. This study mainly aimed to analyze the influence of different aerosol types on the PM_{2.5} estimation. Therefore, we selected a mature statistical model to estimate the PM_{2.5} concentrations, which is defined as follows:

$$\begin{aligned} \ln(\text{PM}_{2.5,\text{st},i}) = & (\alpha + \omega) + (\beta_{1,i} + u_{1,i}) \times \ln(\text{AOD}_{\text{st},i}) + (\beta_{2,i} + u_{2,i}) \times \text{TMP}_{\text{st}} \\ & + (\beta_{3,i} + u_{3,i}) \times \text{RH}_{\text{st}} + (\beta_{4,i} + u_{4,i}) \times \ln(\text{PBLH}_{\text{st}}) \\ & + (\beta_{5,i} + u_{5,i}) \times \text{SP}_{\text{st}} (\beta_{6,i} + u_{6,i}) \times \ln(\text{WS}_{\text{st}}) \\ & + (\beta_{7,i} + u_{7,i}) \times \text{WD}_{\text{st}} + \beta_{8,i} \times \text{ELEV}_s + \beta_{9,i} \times \text{Pop}_s + \varepsilon_{\text{st},i} \end{aligned} \quad (1)$$

where PM_{2.5,st,i} are the dependent observation vectors and AOD_{st,i}, TMP_{st}, RH_{st}, PBLH_{st}, SP_{st}, WS_{st}, and WD_{st} are the independent vectors for grid s on day t. ELEV_s and Pop_s are also independent vectors. All parameters are listed in Table 2.

The slope and intercept were calculated by applying the model dataset to Equation (1), and the PM_{2.5} concentrations can be estimated over the region. A ten-fold cross validation (CV) was conducted to assess the performance of the model to avoid overfitting. The theory of CV is that the entire model-fitting dataset is randomly split into 10 subsets, and 10 rounds of model fitting and prediction are completed. Nine subsets are used to fit the model, and the tenth subset is selected as the testing sample. The process is repeated 10 times in turn, and each predicted value is obtained. The mean of all ten times is the result of the CV. To evaluate the goodness of fit of the model, we computed the coefficient of determination (R^2) and root mean square error (RMSE) for both the observed and estimated PM_{2.5} concentrations.

Table 2. Parameters used in this study.

Variable	Unit	Description
i	Unit less	Aerosol type
AOD	Unit less	VIIRS AOD
TMP	°C	Temperature
WS	m/s	Wind speed
WD	°	Wind direction
RH	%	Relative humidity
SP	hPa	Surface pressure
PBLH	m	Boundary layer height
ELEV	m	Elevation
Pop	Ten thousand/km ²	Population density
α	Unitless	Fixed effects intercept
ω	Unitless	Random effects intercept
$\beta_1-\beta_9$	Unitless	Fixed effects slope
$\mu_1-\mu_7$	Unitless	Random effects slope
ε	Unitless	Random errors

3. Results

3.1. Validation of VIIRS AOD

The relationship between ground-measured AOD and VIIRS AOD is presented in Table 3. Overall, the correlation was relatively high, which indicates that the AOD determined by the two methods were consistent with each other. However, the correlations had large differences between sites. For example, the correlation was relatively low at the Shapotou Station, and there was a serious underestimation compared with the ground-measured observations. The R^2 values at Hong Kong and Yantai Stations were low, and were high at the suburban and vegetation-covered dense stations (BJF, BJC_1, Nanjing, etc.). VIIR AOD exhibited good consistency with the ground-measured observations when the AOD was relatively low, but it was overestimated when the AOD was high.

Table 3. The relationship between ground-measured and Visible Infrared Imaging Radiometer Suite Aerosol Optical Depth at each station.

Station	Expression	R^2	RMSE	N
Shapotou	$Y = 0.43 X + 0.01$	0.27	0.32	182
Hongkong	$Y = 0.56 X + 0.33$	0.25	0.29	61
Yantai Coast	$Y = 0.54 X + 0.30$	0.33	0.32	155
Beijing Forest	$Y = 0.72 X + 0.04$	0.52	0.14	180
Xianghe	$Y = 0.65 X + 0.08$	0.64	0.33	279
Yucheng Agriculture	$Y = 0.87 X + 0.33$	0.66	0.28	239
Beijing-City1	$Y = 0.62 X + 0.10$	0.62	0.27	132
Beijing-City2	$Y = 0.77 X + 0.18$	0.66	0.26	198
Nanjing	$Y = 0.97 X - 0.04$	0.59	0.19	43
Qiyanzhou	$Y = 0.78 X + 0.08$	0.48	0.22	67

The accuracy of VIIRS AOD retrieval is different for different surface types, according to Table 3. Therefore, taking into account the feasibility of the data when constructing models, we classified aerosol types into four categories to evaluate the VIIRS AOD accuracy for different aerosol types: dust type, smoke type (smoke-low and smoke-high), urban type (urban-clean and urban-polluted), and uncertain type. Additionally, the “All” category was the unclassified aerosol type, in which the data contained dust, smoke, urban, and uncertain data types. The definition of the uncertain type was that a pixel was identified as different aerosol types when matching the lookup tables. Scatter plots between AODs of different aerosol types and ground-measured data are shown in Figure 2. The retrieval accuracy

of the dust aerosol type was relatively low and the AOD was seriously underestimated, within the range of 0–0.5. A good agreement was found for the smoke aerosol type, and the AOD was evenly distributed from 0–2, although there was a small underestimation when the AOD was high. The AOD of an uncertain aerosol type was mostly concentrated from 0–1. However, the AOD was significantly overestimated when the AOD value was less than 0.5. The urban aerosol AOD (between 0–1.5) was relatively small when compared with the smoke aerosol AOD.

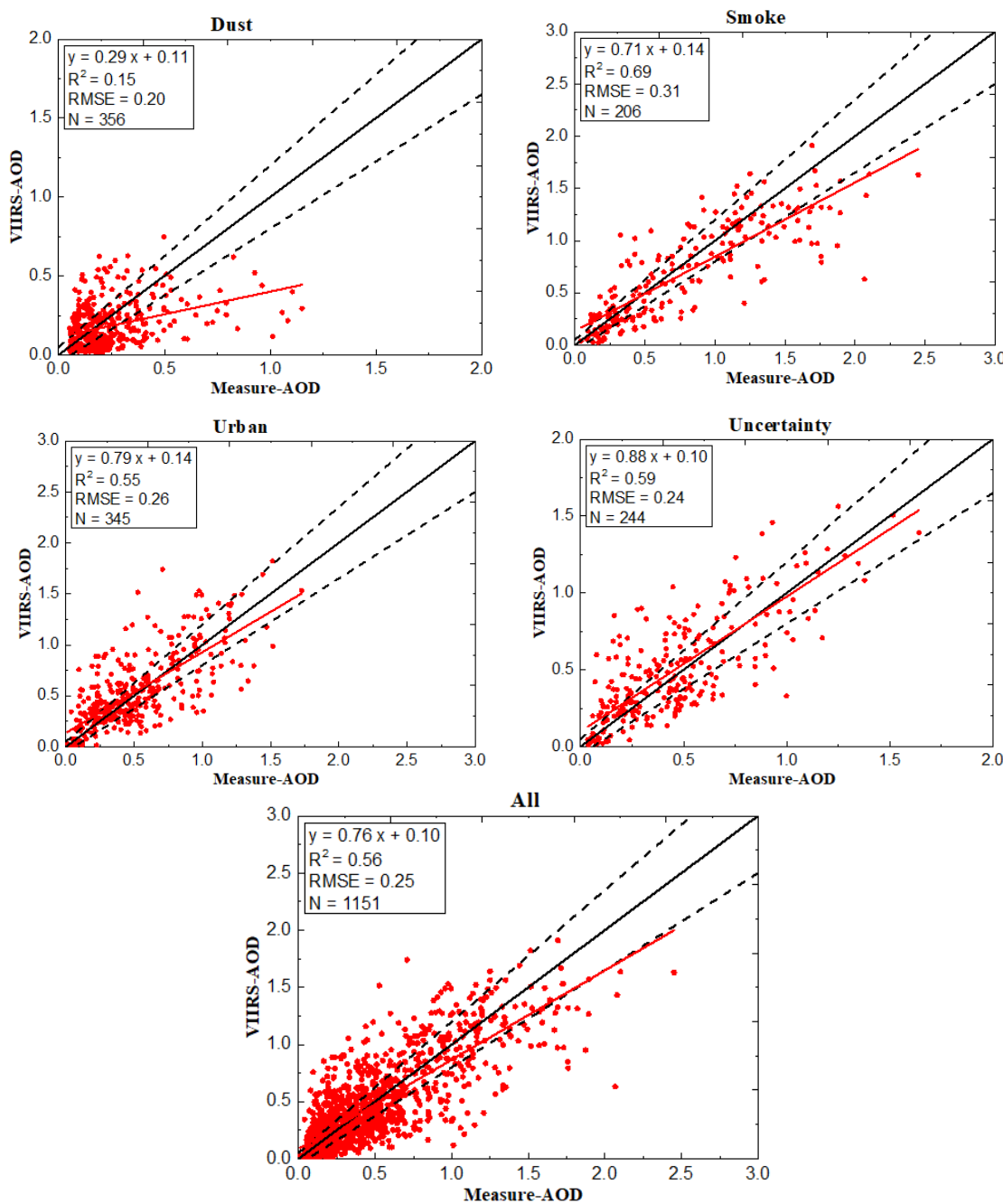


Figure 2. Scatter plots between the different aerosol types of VIIRS AOD and ground-measured AOD. The X axis is the ground-measured, and the Y axis is the VIIRS AOD.

3.2. Model Fitting and Validation

The AOD accuracy of different aerosol types was not the same, according to Figure 2. Simple linear relationships between AOD and PM_{2.5} were calculated for 2015 and 2016, as indicated in Table 4. The result shows that the R² between the different aerosol types were not equal, the dust aerosol had the lowest correlation, and the smoke aerosol had the highest correlations.

Table 4. The coefficients of determination between different types of Visible Infrared Imaging Radiometer Suite Aerosol Optical Depth and PM_{2.5}.

Year	Dust	Smoke	Urban	Uncertain	All
2015	0.12	0.27	0.17	0.24	0.16
2016	0.13	0.24	0.16	0.22	0.15

Based on the inconsistent correlation between AOD and PM_{2.5} (Table 4), a model was established for the different aerosol types according to Equation (1) (Method 1) and the unclassified aerosol types (Method 2). Additionally, CV verification was applied to the data to test the potential model overfitting. Taking BTH as an example, the density scatter plots verified by CV are shown in Figure 3. The figure shows an underestimation when the PM_{2.5} concentrations exceeded 200 µg/m³, whereas the scatter plots were evenly distributed when the PM_{2.5} concentrations were relatively low, and the correlation was significantly improved. The dust aerosol only had a few data samples, which could be because most dust aerosols over BTH come from long-distance transmissions from desert regions such as Inner Mongolia during the winter and spring. Except for a few high values of PM_{2.5} (Figure 3b), the scatterplots of smoke aerosol were evenly distributed on both sides of the fitted line. The point distribution of an urban aerosol was more concentrated than that of the uncertain aerosol (Figure 3c,d). The value of the uncertain aerosol was seriously underestimated when PM_{2.5} concentrations exceeded 150 µg/m³. The R² of the unclassified aerosol type (Figure 3e) was greater than that of the dust aerosol, but less than that for the smoke, urban, and uncertain aerosol types. The dust aerosol over the PRD, MYR, SC, and YRD was classified as an uncertain aerosol type to avoid overfitting because of the small amount of data, and the CV results are listed in Table 5.

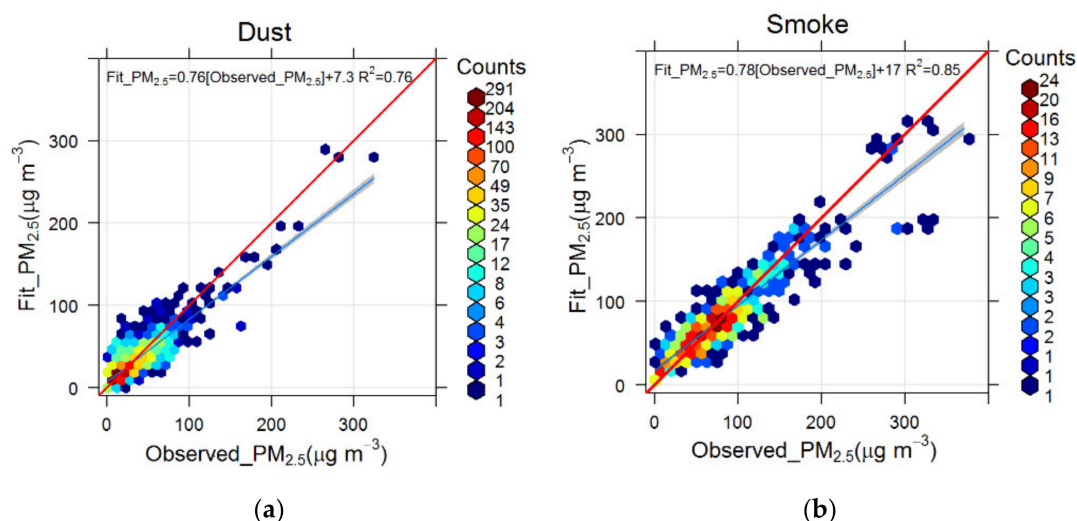


Figure 3. Cont.

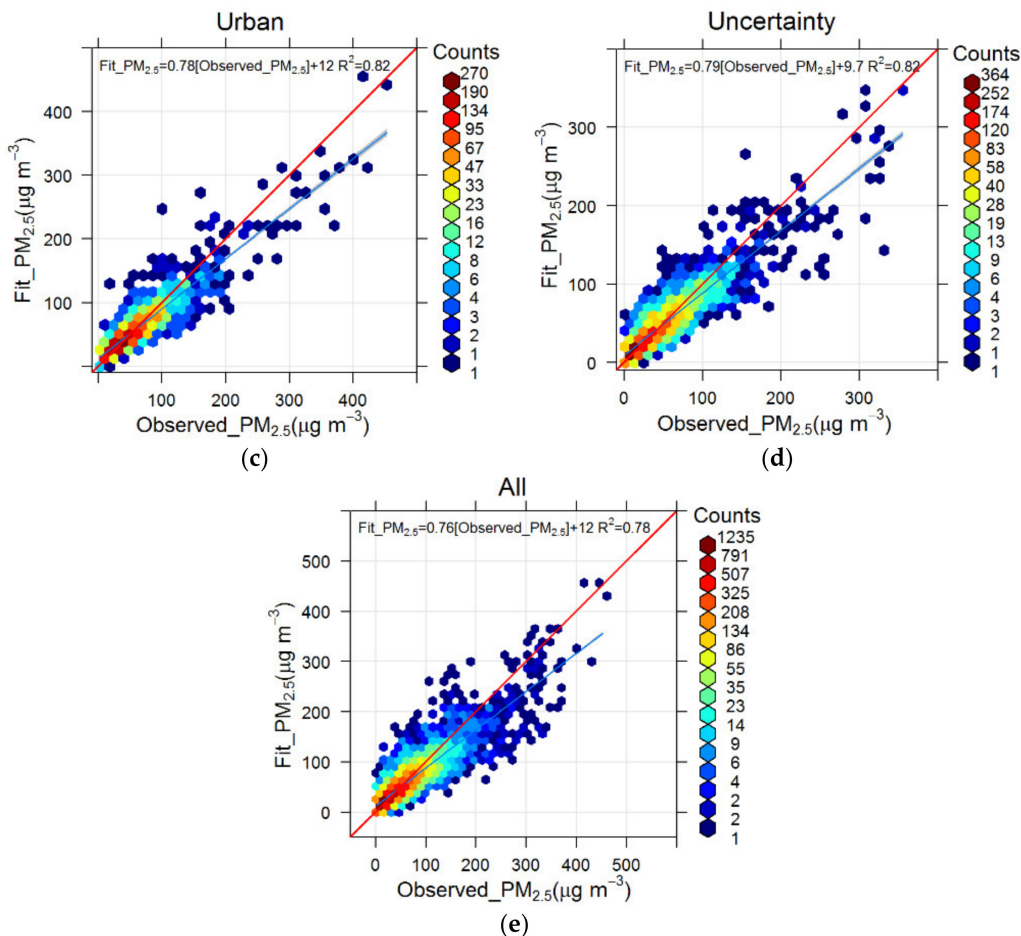


Figure 3. Cross validation of the predicted vs. observed PM_{2.5} concentrations for different aerosol types. (a), (b), (c), (d), and (e) show the dust, smoke, urban, uncertainty, and all, respectively.

Table 5. Parameters of cross validation for the model in Sichuan–Chongqing (SC), Pearl River Delta (PRD), Yangtze River Delta (YRD), and Middle Yangtze River (MYR)

Location	Value	All	Smoke	Urban	Uncertain
PRD	R ²	0.76	0.83	0.83	0.78
	RMSE ($\mu\text{g}/\text{m}^3$)	8.7	9.6	7.95	7.83
MYR	R ²	0.73	0.77	0.79	0.75
	RMSE ($\mu\text{g}/\text{m}^3$)	15.01	9.47	16.3	13.55
SC	R ²	0.79	0.83	0.83	0.79
	RMSE ($\mu\text{g}/\text{m}^3$)	14.45	11.36	14.31	13.08
YRD	R ²	0.80	0.89	0.85	0.81
	RMSE ($\mu\text{g}/\text{m}^3$)	12.58	9.61	12.31	10.80

The CV R² of the urban aerosol was greater than that for smoke aerosol, except for the YRD. The CV R² (RMSE) of the classified aerosol type was greater (less) than that of the unclassified aerosol type. The CV R² of the smoke and urban aerosol was greater than that of the uncertain aerosol type, and the uncertain aerosol type thus had a certain impact on the PM_{2.5} estimation accuracy. After the above analysis, constructing models for different aerosol types helps to improve the PM_{2.5} estimation accuracy.

3.3. Comparison of $PM_{2.5}$ Daily Estimates

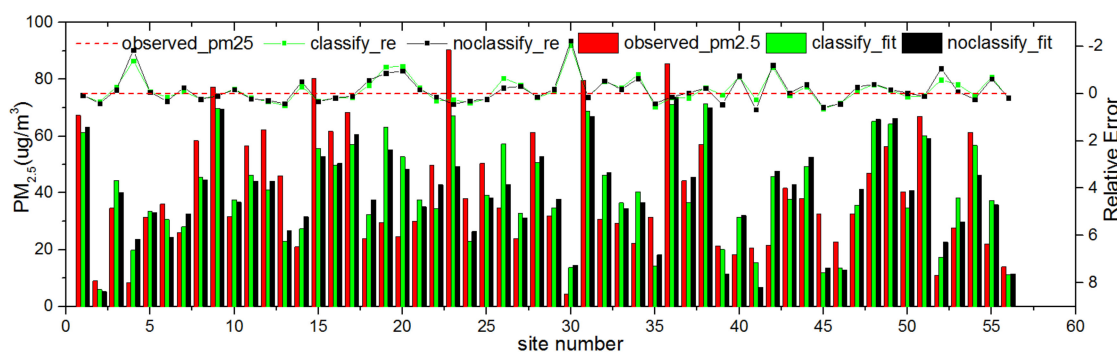
The data from the clear and minimal cloud coverage conditions were selected from 2015 to 2016, and the PM_{2.5} pollution levels were classified according to the national standards. The air quality

level differences were compared between the satellite-retrieved data and ground-measured data, and the accuracy of the PM_{2.5} satellite retrieval was quantitatively analyzed. The r and RMSE between the ground-measured and satellite-estimated over five regions were calculated and are reported in Table 6. The relative errors ($RE = (\text{Ground-measured} - \text{Satellite})/\text{Ground-measured}$), the PM_{2.5} estimation results (both methods), and ground-measured data at each station are shown in Figure 4. According to the list of histograms, the estimation of PM_{2.5} via the classified method was closer to the ground-measured data, and the REs were less so, when using the classified aerosol types compared with the unclassified aerosol type (except for a few sites). Meanwhile, the statistics of the REs showed that more than 60% of the data fell within $\pm 30\%$ in BTH, more than 80% of the data fell within $\pm 30\%$ in SC, approximately 97% (88%) fell within $\pm 30\%$ (20%) in PRD, approximately 80% as within $\pm 30\%$ in YRD, and approximately 92% (75%) were within $\pm 30\%$ (20%) in MYR.

To analyze the spatial distribution of PM_{2.5}, the data selected are shown in Figure 5. In the air quality grades, the distribution of PM_{2.5} grades estimated using the classified aerosol type method was generally more consistent with the ground-measured observations. For example, the PM_{2.5} values of some stations in Shijiazhuang and Tangshan, based on the classified aerosol type, were closer to the ground-measured data than those based on the unclassified aerosol type in BTH. In SC, the result obtained using the classified aerosol type method could articulate more detailed information, while the unclassified aerosol type method did not show the differences among different regions compared to the ground-measured PM_{2.5}. In PRD, the estimation result using the unclassified aerosol type method was seriously overestimated in some regions such as Jiangmen and Zhongshan. The spatial distributions of PM_{2.5} in the YRD and MYR exhibited little differences between the classified and unclassified aerosol type methods. On 6 December, 2016, heavy and serious pollution areas were mainly located west of Jiujiang and Yichun, but Xinyang had better air quality. Overall, although some were overestimated or underestimated using the satellite estimation method, it was obviously advantageous in determining the spatial distribution and could contribute to the evaluation of air quality on the macro level.

Table 6. Statistical parameters for the ground-measured and satellite-estimated values in Beijing–Tianjin–Hebei (BTH), Sichuan–Chongqing (SC), Pearl River Delta (PRD), Yangtze River Delta (YRD), and Middle Yangtze River (MYR)

Regions	Time	Classified		Unclassified	
		r	RMSE ($\mu\text{g}/\text{m}^3$)	r	RMSE ($\mu\text{g}/\text{m}^3$)
BTH	2016-05-10	0.76	11.0	0.73	11.1
SC	2015-10-14	0.80	16.45	0.75	19.65
PRD	2015-01-18	0.75	6.34	0.65	13.8
YPD	2015-10-12	0.73	9.15	0.71	12.85
MYR	2016-12-06	0.94	10.98	0.92	12.54



2016-05-10 Beijing–Tianjin–Hebei (BTH)

Figure 4. Cont.

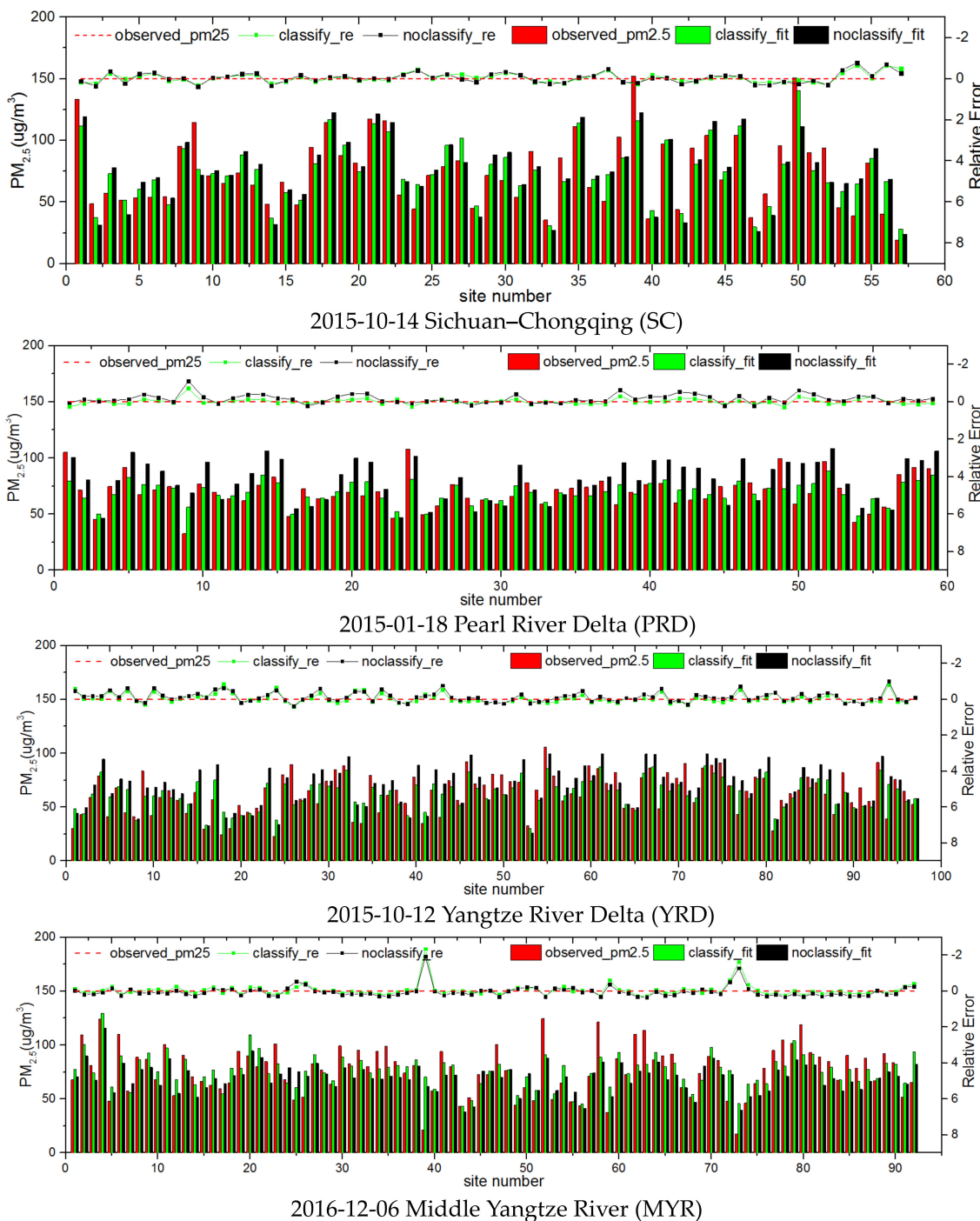
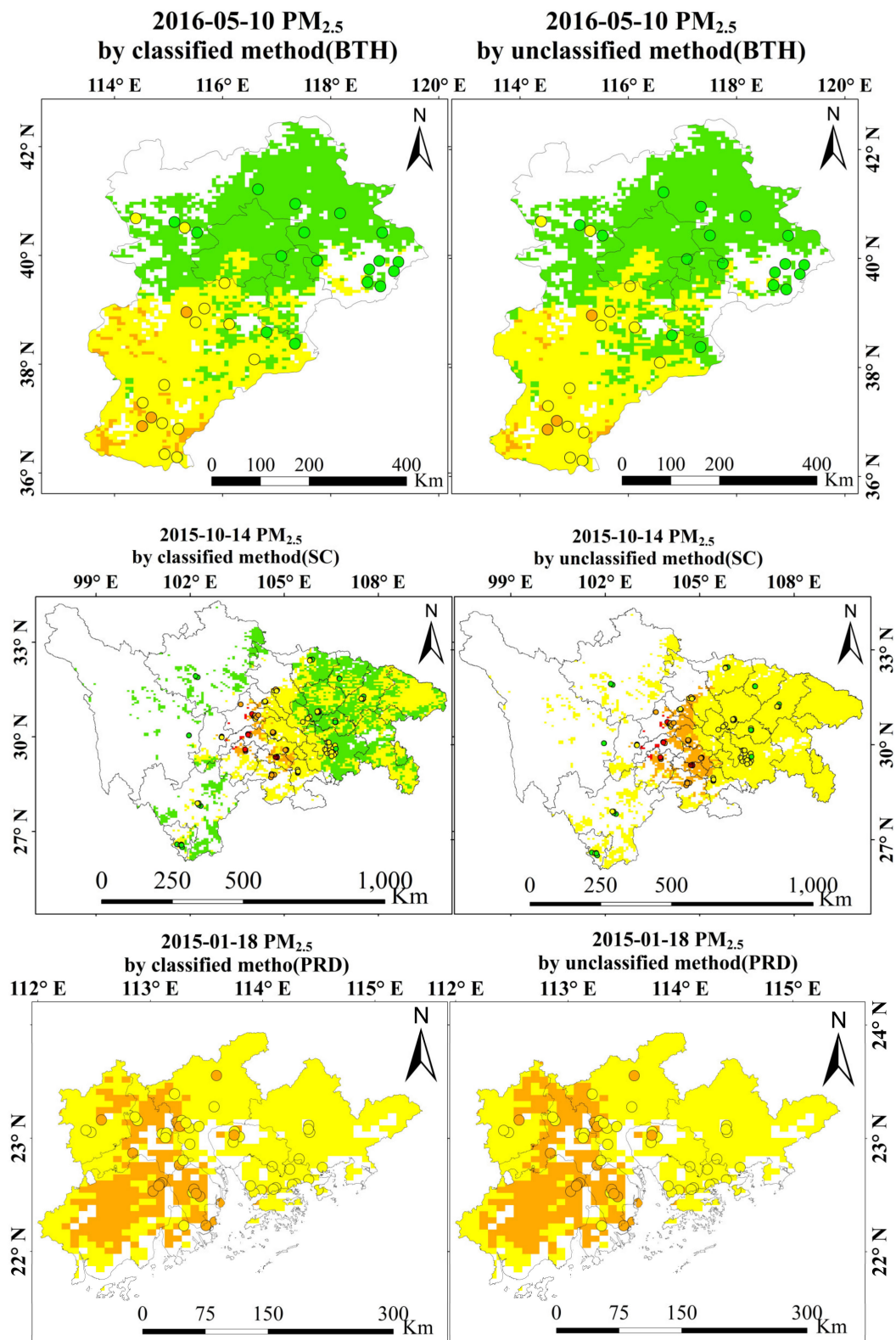


Figure 4. The relative error (RE) in the PM_{2.5} concentrations for the ground-measured and satellite retrieval result using the classified and unclassified aerosol type methods in Beijing–Tianjin–Hebei (BTH), Sichuan–Chongqing (SC), Pearl River Delta (PRD), Yangtze River Delta (YRD), and Middle Yangtze River (MYR). The red dashed, green solid, and dark lines are the RE values calculated via ground-measured, classified, and unclassified methods. The red, green, and dark rectangles are the PM_{2.5} obtained using the ground-measured, classified, and unclassified methods, respectively.

**Figure 5. Cont.**

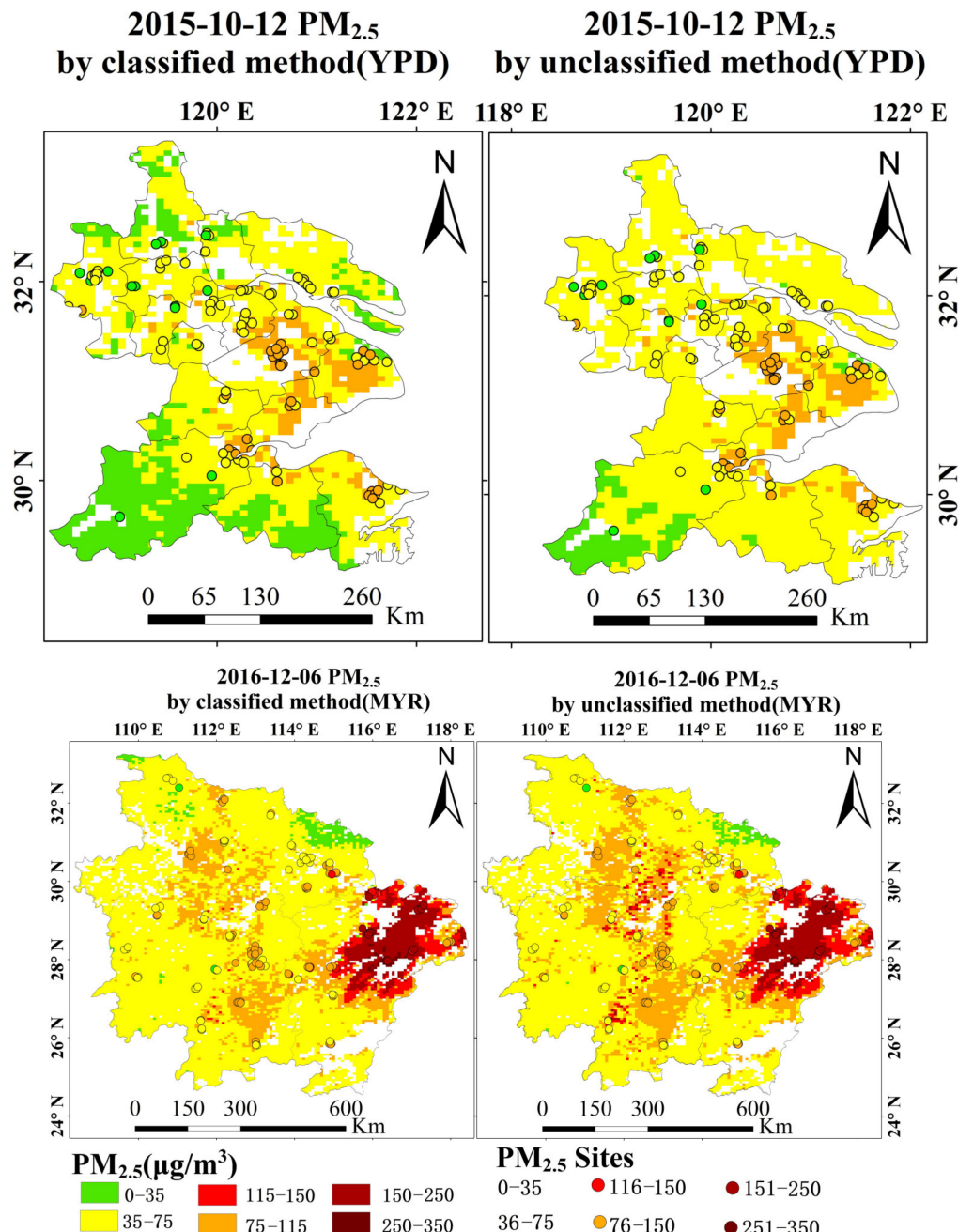


Figure 5. The distributions of PM_{2.5} obtained using the classified and unclassified aerosol type methods in Beijing–Tianjin–Hebei (BTH), Sichuan–Chongqing (SC), Pearl River Delta (PRD), Yangtze River Delta (YRD), and Middle Yangtze River (MYR).

3.4. Spatiotemporal Variations in Satellite-Retrieved PM_{2.5}

The estimation results obtained using the two methods suggest that satellite remote sensing technology is a simple but effective means to estimate the regional PM_{2.5} concentrations, especially for some areas with sparse ground-measurement stations. To analyze the PM_{2.5} variations for heavily polluted areas in China from 2015 to 2016, the spatiotemporal distributions of the PM_{2.5} estimates based on the classified aerosol type method in BTH, SC, YRD, MYR, and PRD are shown in Figures 6–10.

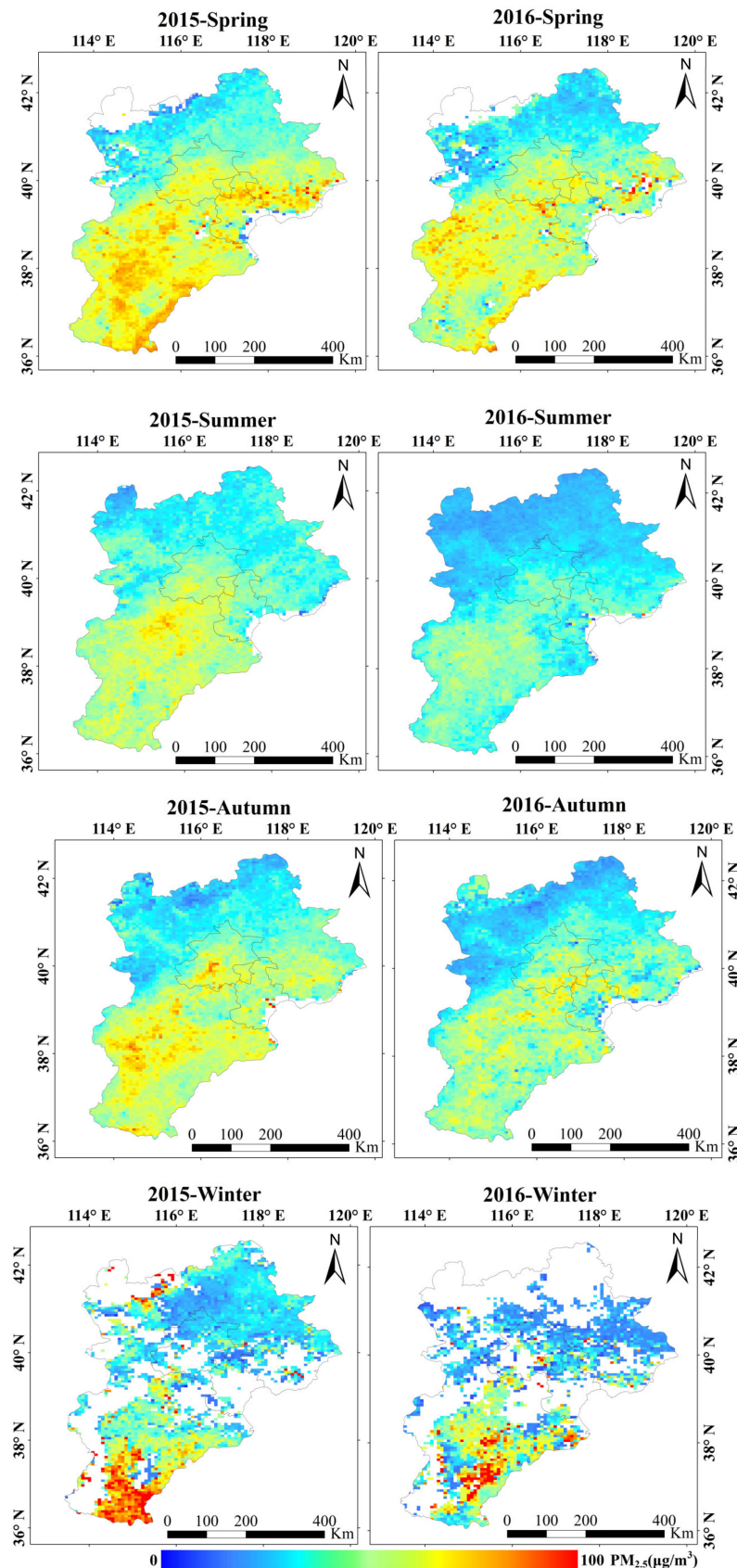


Figure 6. Spatiotemporal distributions of PM_{2.5} concentrations in Beijing–Tianjin–Hebei BTH.

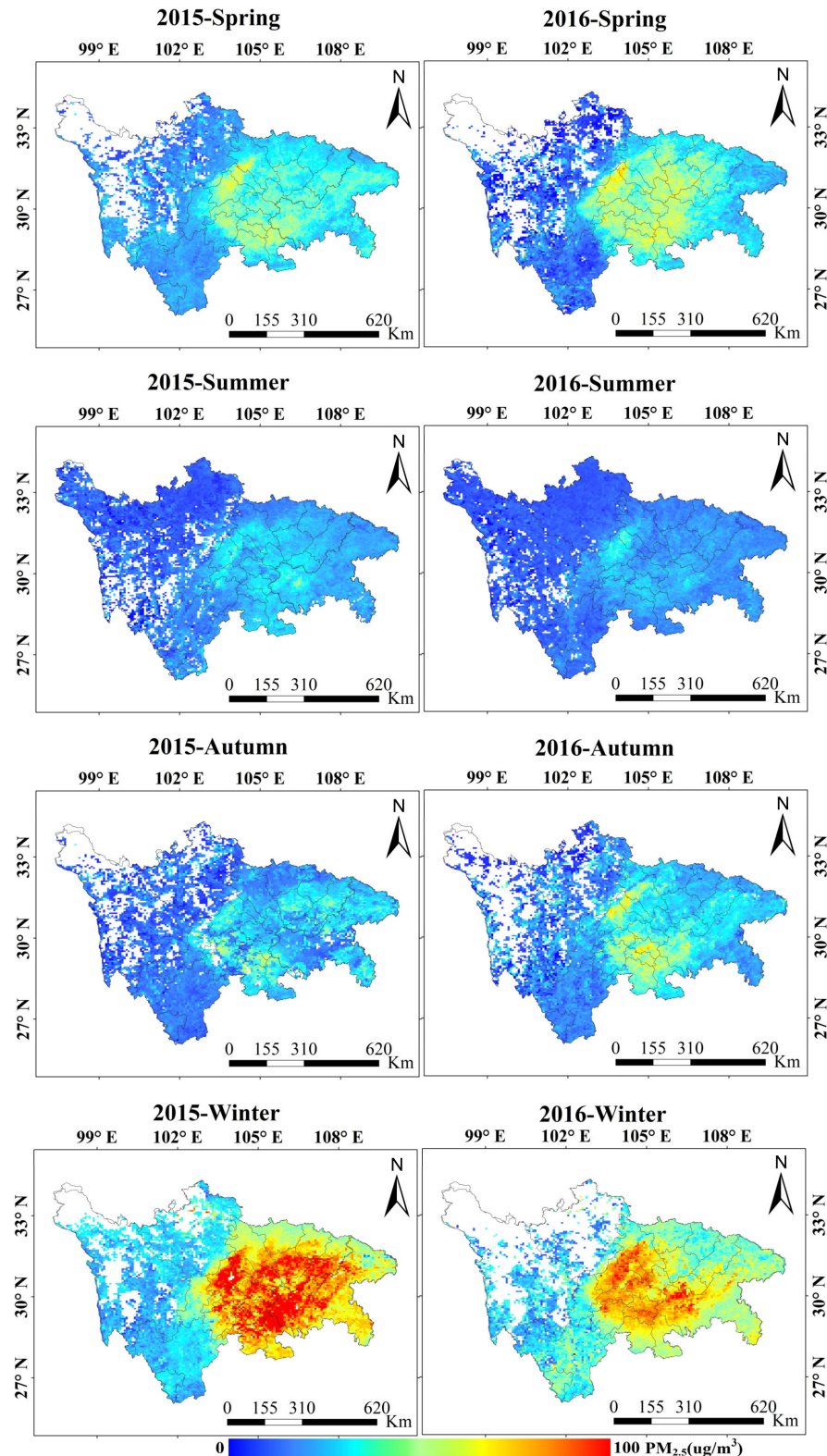


Figure 7. Spatiotemporal distributions of PM_{2.5} concentrations in Sichuan–Chongqing (SC).

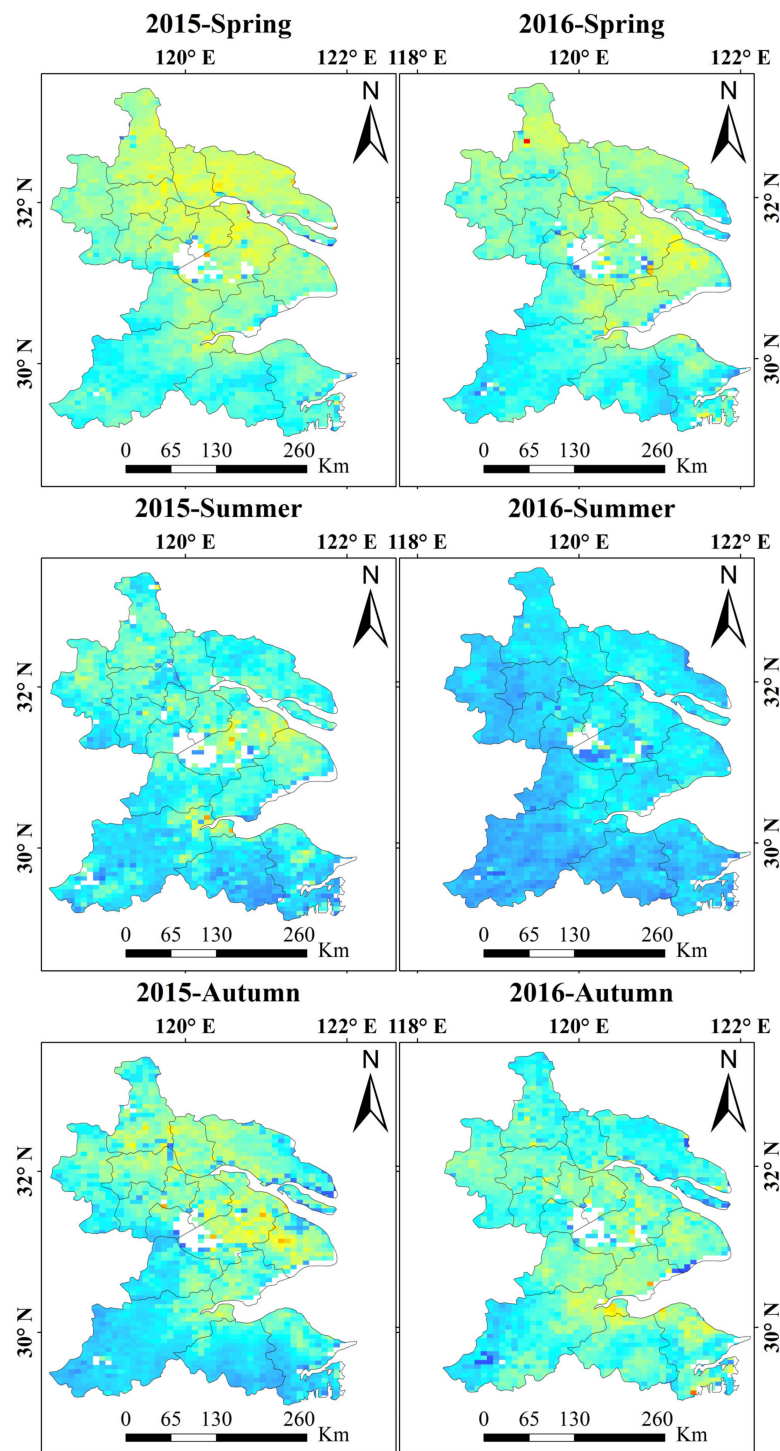


Figure 8. Cont.

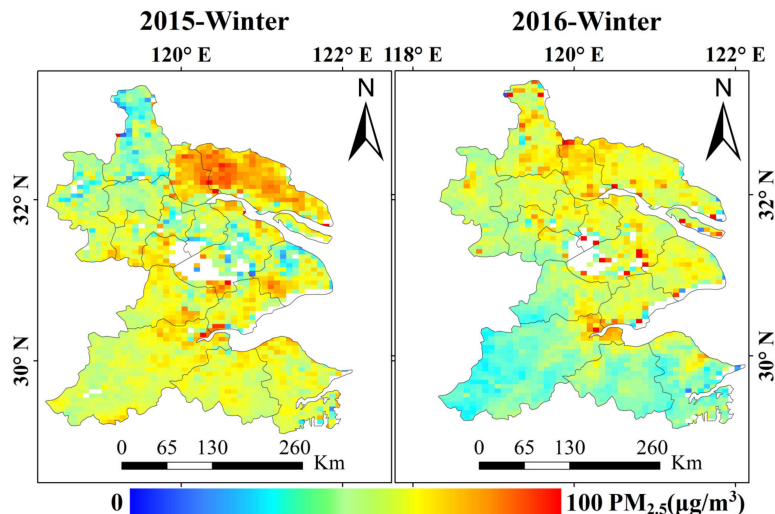


Figure 8. Spatiotemporal distributions of PM_{2.5} concentrations in the Yangtze River Delta (YRD).

(1) Beijing–Tianjin–Hebei (BTH)

Figure 6 shows the seasonal variations in PM_{2.5} as estimated with the aerosol type method and VIIRS AOD in BTH during January 2015 to December 2016. The spatial distributions exhibit a strong south-to-north increasing gradient, which is mainly related to the topography, weather conditions, land cover types, and emission sources. The Taihang Mountains west of Hebei Province inhibit pollutant dispersion, which leads to pollutant accumulation in the North China Plain. Heavy pollution areas are located in southern and urban regions with lower vegetation coverage, higher pollution density, and lower topography. Northwest of the mountainous region is an area of good air quality with denser vegetation cover, less population, and higher topography. The PM_{2.5} concentrations in the southern Hebei Province were higher than those in Beijing and Tianjin because of the large amount of industrial pollution, and the air quality was thus poor. According to the ground observations, the pollutants are released into the air due to heating in winter, and poor weather conditions are not conducive to pollutant diffusion in BTH, which leads to high PM_{2.5} concentrations. However, the satellite-retrieved data did not reflect the high PM_{2.5} concentrations in winter, which is related to the lack of high-quality AOD data. The seasonal variations were consistent with the ground measurements, and the concentrations of PM_{2.5} were the highest in winter and lowest in summer. During summer, the prevailing unstable atmospheric conditions and precipitation are conducive to pollutant diffusion, and the air quality is better. The seasonal average concentrations of PM_{2.5} are higher in spring due to the influence of dust, and in autumn due to straw and coal burning for heating in November. Compared with 2015, in 2016, the seasonal average concentrations of PM_{2.5} in BTH decreased, and the air quality improved.

(2) Sichuan–Chongqing (SC)

Figure 7 shows the seasonal distribution of PM_{2.5} in both 2015 and 2016 over SC. Spatially, the high PM_{2.5} concentrations were located in the city clusters of the Sichuan Basin (SB), and the air quality was better in the western Sichuan Plateau, which could be attributed to the following reasons. First, the city clusters of the SB are densely populated, and the discharge of a large amount of vehicle exhaust and industrial pollutants will lead to higher PM_{2.5} concentrations. Second, the SB is located southeast of the Tibetan Plateau at a low altitude and is surrounded by mountains; therefore, unfavorable topography and climatic conditions inhibit the diffusion of pollutants. Third, the western Sichuan Plateau has a high elevation, a sparse population, dense vegetation coverage, and fewer pollution sources, which create better air quality [47]. Regarding seasonal variations, the PM_{2.5} concentrations were the highest during winter and lowest during summer, and the second-highest concentrations

occurred during spring and autumn. The main reason is that the lower PBLH is dry with little rainfall, which easily leads to the inversion of temperature and the accumulation of pollutants in the bottom layer of the atmosphere, which is not conducive to the diffusion of pollutants during spring and winter [48]. In summer and autumn, the temperature and humidity are high in PBLH during summer, which is conducive to the diffusion of pollutants and thus the lowest PM_{2.5} concentrations. In 2016, the concentrations of PM_{2.5} decreased in winter but increased in the southwestern SB in autumn and spring compared with 2015, consistent with the results of Zhao et al. [47]

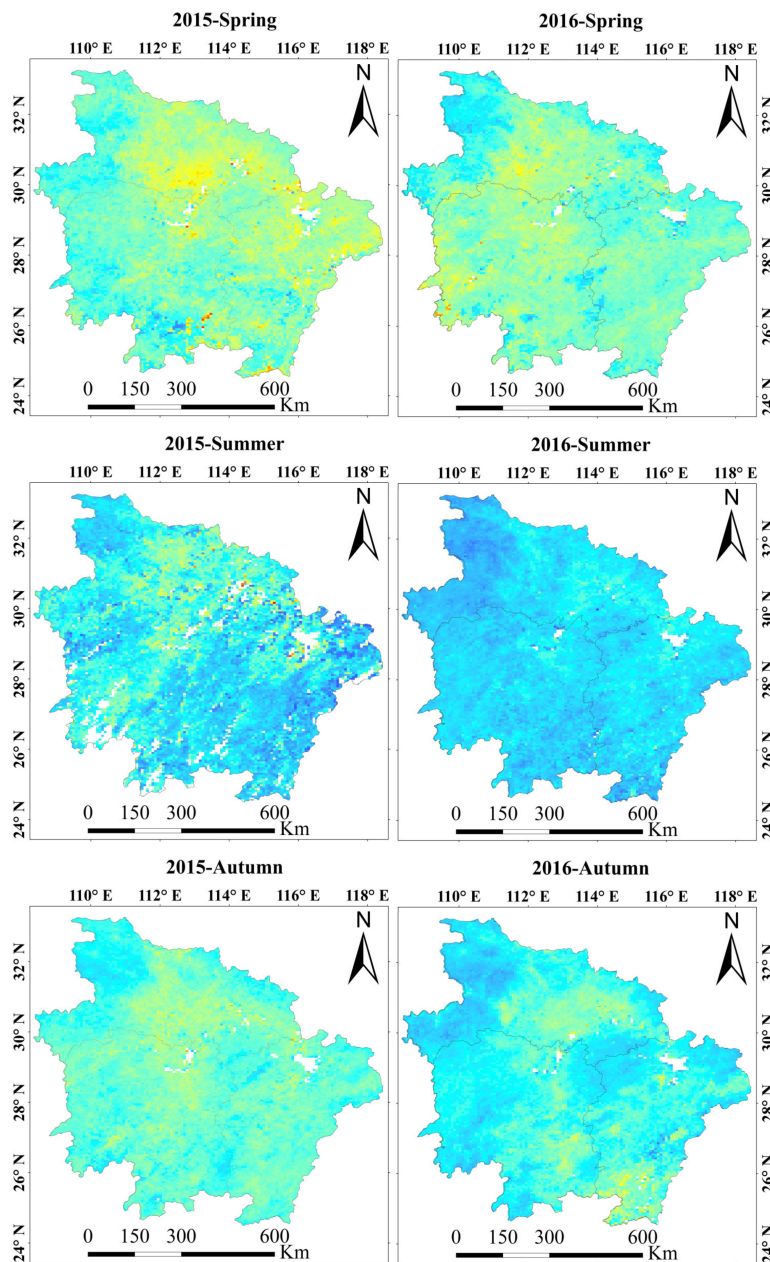


Figure 9. *Cont.*

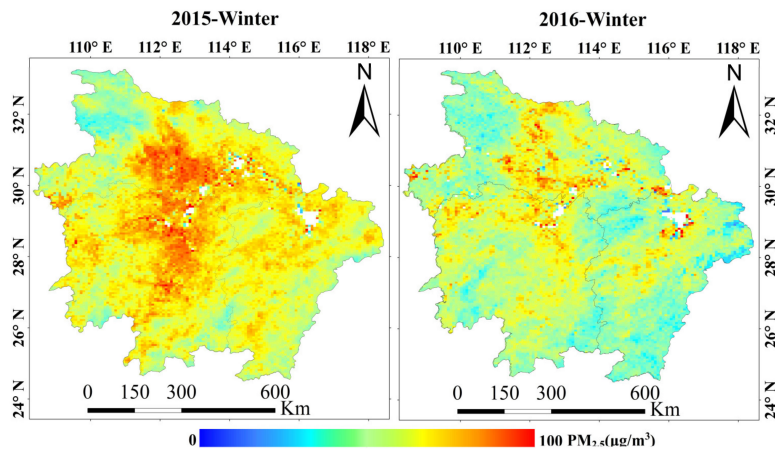


Figure 9. Spatiotemporal distributions of PM_{2.5} concentrations in the Middle Yangtze River (MYR).

(3) Yangtze River Delta (YRD)

The seasonal and spatial variations in PM_{2.5} in 2015 and 2016 are shown in Figure 8. The spatial distributions exhibit a strong north-to-south decreasing gradient. The high PM_{2.5} concentrations were mainly located in city clusters such as Shanghai, Suzhou, and Wuxi, where the generation of aerosols due to human activities is larger and large amounts of pollutants (from industrial sources, vehicle exhaust, road dust, and other sources) are released into the atmosphere, leading to high PM_{2.5} concentrations. There is better air quality south of the YRD, where the vegetation cover is dense, human activity and pollution sources are relatively less, and the dense vegetation can block some surface particles from entering the atmosphere. The seasonal variation in PM_{2.5} concentrations showed an obvious pattern, winter > spring > autumn > summer, which agreed well with the conclusions by He et al. [27]. In winter, the PM_{2.5} concentrations in the YRD are affected by the air flow transmission carrying pollutants from north and east China. The dominant source of PM_{2.5} in the YRD is the secondary reactions of sulfur, nitrogen, and ammonia emissions from industry, coal, vehicles, and dust. Therefore, the following climatic conditions that prevail in the downdraft result in difficulties in spreading the local pollutants, and the PM_{2.5} concentrations are high in winter. As the East Asian monsoon and mainly northwesterly winds prevail over the YRD in the spring, some of the large-diameter dust aerosols are transmitted by the monsoons from the north, which leads to higher PM_{2.5} concentrations than in the autumn; however, the difference is small [49]. In summer, the strong atmospheric motion is conducive to pollutant diffusion, and heavy rainfall promotes the wet deposition of particles to reduce pollutant concentrations in the atmosphere [50]. Simultaneously, the clean air provided by the ocean monsoon transmitted via the Pacific Ocean has a strong dilution effect on air pollution and thus reduces the PM_{2.5} concentrations in the atmosphere [51]. The PM_{2.5} concentrations in most cities of the YRD decreased in 2016 compared with 2015. However, in the winter of 2016, the PM_{2.5} concentrations in some cities such as Shanghai, Suzhou, and Wuxi were relatively high. This was mainly because the area experienced four periods of high-concentrations and large-scale and long-term particle pollution in December 2015, which was influenced by the long-distance transport of the southwest and northern air currents [52].

(4) Middle Yangtze River (MYR)

The MYR is also one of the most heavily polluted areas according to the statistical analysis of the national PM_{2.5} concentrations. The spatiotemporal distributions of PM_{2.5} concentration during 2015–2016 are shown in Figure 9. The high PM_{2.5} concentrations were mainly concentrated southwest of Hubei and northeast of Hunan. The PM_{2.5} concentrations in Hubei had a unique spatial distribution. The PM_{2.5} concentrations were the highest in the central regions (such as Jingmen, Tianmen, and Qianjiang) and lowest in the western regions (such as Enshi and Shiyan), and concentrations in the

eastern regions were higher than in the western regions (such as Huangshi). The unique distribution might be explained by the mountains surrounding the eastern, western, and northern sides of Hubei Province; the center is low-lying, and the incomplete basin is slightly open to the south, which forms two transmission channels of pollutants (Xiangyang–Jingmen–Jingzhou and Suizhou–Xiaogan–Wuhan). Therefore, the PM_{2.5} accumulated in the central area, and the eastern and western areas were relatively low [53]. In the cities of Changsha, Zhuzhou, Xiangtan, and Changde, which are Hunan's economic development centers, industrial and vehicle emissions led to relatively high PM_{2.5} concentrations. Jiangxi Province had higher PM_{2.5} concentrations in Nanchang and Yichun. The seasonal distribution of PM_{2.5} concentrations in MYR had similar characteristics in 2015 and 2016: winter > spring > autumn > summer [54]. This distribution could be explained by the following two factors. First, the MYR is located in southern China, where the temperature is high, and heavy rainfall directly removes atmospheric particulates in summer. Moreover, heavy rainfall increases the humidity in the air, which helps to increase the mass and viscosity of the particulate matter and accelerate the wet deposition of PM_{2.5} particulate matter, which reduces the pollutants in the air. However, the temperature is relatively low in the winter, and the rainfall is relatively little. The discharge of pollutants increases with heating, which leads to higher concentrations of PM_{2.5}. Second, in summer, the southeast wind prevails, and the WS is relatively high, which are both conducive to the diffusion of pollutants. The northerly wind prevails, carrying some pollutants from the north to the MYR, which increases the concentration of pollutants in winter and is not conducive to the diffusion of pollutants.

(5) Pearl River Delta (PRD)

According to the spatiotemporal distributions of PM_{2.5} in the PRD from 2015 to 2016 (Figure 10), the PM_{2.5} concentrations were relatively low when compared with BTH, SC, YRD, and MYR, which could be attributable to two factors. First, to hold the 16th Annual Asian Games in 2010, many factories were forced to control PM_{2.5} concentrations through various means such as the closure or relocation of heavily polluting factories. Second, the PRD is located in the southernmost part of China and is close to the sea. Heavy rainfall occurs frequently, which is conducive to the removal of pollutants. The PM_{2.5} concentrations around Guangzhou and Foshan were higher than in other regions because of the high emission of fuel sources and vehicles located in urban centers. In the PRD, PM_{2.5} is mainly formed by the secondary conversion of gas precursors such as sulfur dioxide and nitrogen oxides, which results in high PM_{2.5} concentrations. The PM_{2.5} concentrations were high in winter, but low in summer. The PRD is mainly affected by the inland and Fujian coastal air masses, northerly winds, and little rainfall, which lead to the poor performance of atmospheric diffusion and air mass cleanliness in winter. Most of the air masses that reach the PRD in summer come from the clean air masses of the China Sea and South Pacific; the heavy rainfall promotes the wet deposition of particulate matter, thus the PM_{2.5} concentrations are low.

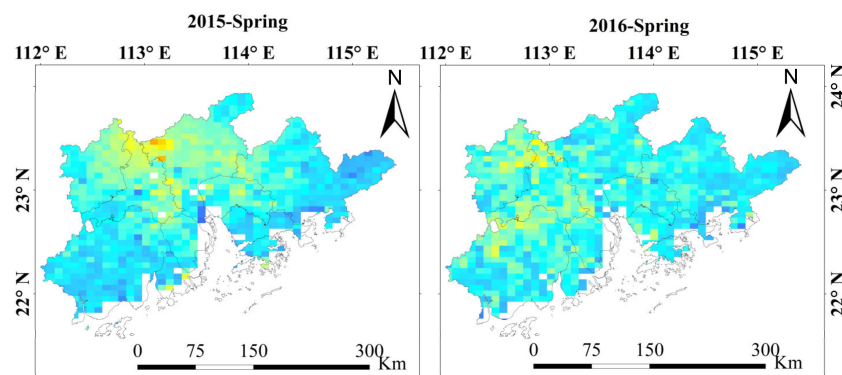


Figure 10. Cont.

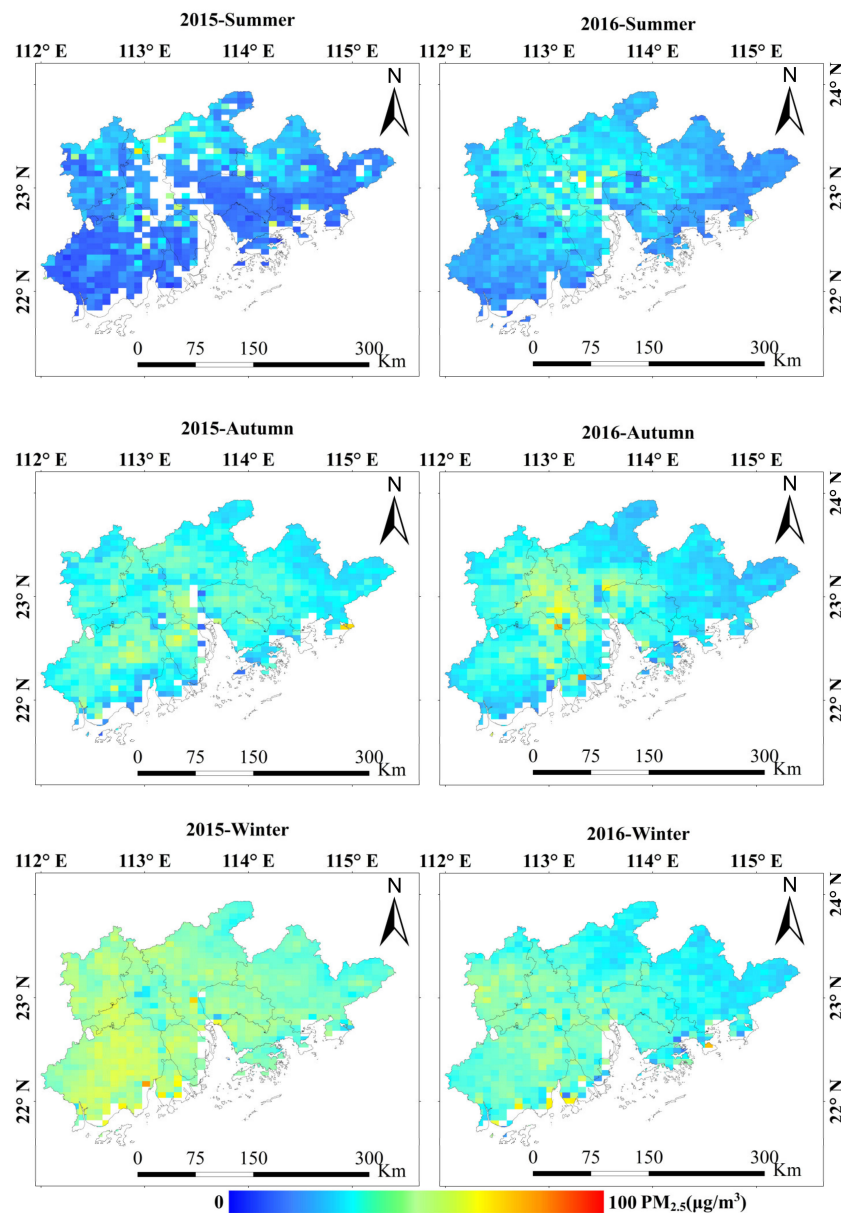


Figure 10. Spatiotemporal distributions of PM_{2.5} concentrations in the Pearl River Delta (PRD).

4. Discussion

Satellite data have been proven to have the capacity to estimate spatiotemporal PM_{2.5} concentrations in areas with few ground measurements such as suburbs. The particle compositions are not the same in different regions, which leads to inaccuracy of the PM_{2.5} estimation. In this study, we first obtained ground-measured AODs to evaluate the accuracy of VIIRS AOD retrieval for different aerosol types and found large differences among the different aerosol types. The dust aerosol type had the lowest correlation, which could be because the algorithm used to retrieve VIIRS AOD adopts the 6SV to construct a lookup table; this process only assumes the scattering function of spherical particles and does not well reflect the characteristics of nonspherical particles. In addition, in the case of dust (and thus also in the case of longer-range transported particles), the variability of the aerosol distribution, especially in the vertical dimension, is higher, and so the AOD–PM_{2.5} relationship can work less well than for local aerosol types. The correlation of salt aerosols is relatively low, and it could be that most of the sea salt particles are coarse and mixed, which would impact the retrieval of AOD over land. The verification results are consistent with Tian's research [55], which used the

Cloud-Aerosol Lidar and Infrared Pathfinder Satellite Observation (CALIPSO) data to analyze the different aerosol types in different regions.

The relationship between PM_{2.5} and AOD has been discussed by many researches; however, these studies have mainly focused on exploring new models or finding new variables related to PM_{2.5} to improve the performance of PM_{2.5} estimation. However, aerosol types have been less discussed in the use of satellite data, perhaps because it is difficult to obtain accurate aerosol types at a large regional scale due to rapid changes in particle composition. Therefore, with the aerosol types given in VIIRS AOD, we proposed a classified aerosol type method to estimate PM_{2.5}. Moreover, our main objective in this study was to explore the performance of using the classified aerosol type method to estimate PM_{2.5}, and we thus selected a mature statistical model. More advanced and complex models (e.g., artificial neural networks, random forests, and support vector machines) will be used to estimate PM_{2.5} in the future.

The models were constructed for dust, smoke, urban, uncertain, and “All” type categories in five different regions to demonstrate the statistical applicability of the method. The CV R² of dust aerosols was the lowest, which is related to the accuracy of AOD retrieval. The CV R² values of smoke, urban, and uncertain aerosol types were greater than that of the “All” type (unclassified aerosol type), which shows that the classified aerosol type performed better in determining the relationship between AOD and PM_{2.5} than the unclassified aerosol type. This result was similar to that from the research of Chen et al. [31]. Although the research by Chen had higher accuracy based on ground measurements, it was spatially and temporally limited because there were fewer and unevenly distributed ground-measurement stations and the data needed to be further processed to distinguish different aerosol types, generating high costs. Therefore, the method proposed in this study is more suitable for long time periods and large spatial regions.

We compared the PM_{2.5} daily estimates, and the results show that the classified aerosol type method was more consistent with the ground-measured observations than the unclassified aerosol type, and the RE was relatively lower. Moreover, compared with the ground-measured observations in Shijiazhuang, in general, the daily average errors were relatively low. However, the RE at some stations was larger and higher with the classified aerosol type method than with the unclassified aerosol type, which can be attributed to two factors. First, the AOD accuracy could be affected by clouds because the edges of the clouds are not cleanly removed, which can lead to large errors in PM_{2.5} estimation. Second, the assumed optical properties used by VIIRS aerosol retrieval were taken from Dubovik et al. (2002) [56], where data from only twelve stations were used. This parameter information thus might not fully represent the aerosol characteristics in China, which could lead to an inaccurate identification of the aerosol types. Therefore, it is critical to obtain accurate aerosol types and AODs to improve PM_{2.5} concentrations.

In addition, according to the distribution of PM_{2.5} in BTH, the lack of data is very serious in winter, which is related to the AOD data. VIIRS AOD is retrieved by the dark pixel algorithm; the vegetation coverage is sparse in the north during winter, which leads to less data availability. On the other hand, the surface reflectance of the nonvegetated areas is estimated to be quite different under heavy haze conditions, and parts of the data are thus classified as non-high-quality products to ensure the high-precision data quality of the AOD.

5. Conclusions

The accuracy of the PM_{2.5} concentrations obtained from ground measurements was high, but the distribution of the sites was uneven, and the number was limited; that is, most nonurban areas have fewer observations than needed to effectively estimate the regional PM_{2.5} concentrations. In contrast, based on the satellite remote sensing technology used to retrieve the AOD with high spatial resolution and continuous coverage characteristics, the relationship established between the AOD and PM_{2.5} can be used to estimate PM_{2.5} concentrations. In this study, based on the characteristics of different aerosol

types, the VIIRS AOD was used to estimate PM_{2.5} concentrations via the classified and unclassified aerosol type methods, and the following conclusions were obtained:

- (1) Using the ground-measured AOD to verify the accuracy of the VIIRS AOD (Figures 1 and 2), the correlation was high ($R^2 > 0.5$) in dense-vegetation-coverage regions, and the correlation with mixed dust or sea salt particles was low ($R^2 < 0.3$). The accuracy of retrieval for different aerosol types was discussed, and the correlation of the smoke (dust) aerosol was the highest, with $R^2 = 0.69$ (lowest $R^2 = 0.15$).
- (2) The linear relationships between the four different aerosol types of AOD and PM_{2.5} in 2015 and 2016 were calculated. The smoke aerosol correlation was the highest (R^2 values of 0.27 and 0.24, respectively), but was greatly improved after construction of the model estimates (Figure 3 and Table 5). The CV R^2 was relatively low for dust aerosols and high for smoke and urban aerosols based on the two methods used to estimate the PM_{2.5} concentrations in BTH, SC, YRD, MYR, and PRD. The uncertain aerosol type had a certain influence on the accuracy of PM_{2.5} estimation.
- (3) The spatiotemporal distribution of PM_{2.5} from 2015 to 2016 was analyzed in BTH, SC, YRD, MYR, and PRD, and the regional PM_{2.5} concentrations were relatively low in the PRD. Spatially, high PM_{2.5} concentrations were located in the city clusters and industrially developed areas, and an unfavorable topographic factor resulted in higher PM_{2.5} concentrations. Some regions at high elevations with dense vegetation coverage and less pollution sources had a low PM_{2.5} concentration. Seasonally, the increase in emissions and unfavorable pollutant diffusion climatic conditions led to the highest PM_{2.5} concentrations in winter. The increase in heavy rainfall, higher WS, and unstable boundary layer height are favorable for the wet deposition and diffusion of pollutants, and the PM_{2.5} concentrations were relatively low in summer.

However, in this study, the aerosol type obtained from the VIIRS attributes could have certain limitations in China. If the aerosol type can be accurately discerned, this will help to improve the accuracy of PM_{2.5} estimation.

Author Contributions: Q.Z. proposed the method, collected data, and wrote this paper; L.C. and J.T. revised the paper; H.Z., S.Z., and Y.W. analyzed the data. All authors have read and agreed to the published version of the manuscript.

Funding: National Magnetic Confinement Fusion Program of China (No. 2017YFB0503901) and the National Magnetic Confinement Fusion Program of China (No. 2016YFC0200404).

Acknowledgments: This study was supported by the National Key Research and Development Program of China (Grant No. 2017YFB0503901; No. 2016YFC0200404) and the National Natural Science Foundation of China (Grant No. 41571347). The authors are grateful to the China Meteorological Data Sharing Service System (<http://data.cma.cn/>), NASA (<https://pmm.nasa.gov/>), CMDSSS (<http://data.cma.cn/>), SRTM (<http://srtm.cgiar.org/>), the European Center (<http://www.ecmwf.int/>), CNEMC (<http://106.37.208.233:20035/>), AERONET (<http://aeronet.gsfc.nasa.gov/>), the Data Center for Resource and Environmental Sciences, and the Chinese Academy of Sciences (<http://www.resdc.cn>) scientific team for the provision of satellite data and in situ measurement data used in this study.

Conflicts of Interest: The authors declare no conflicts of interest.

References

1. Wu, J.; Zhu, J.; Li, W.; Xu, D.; Liu, J. Estimation of the PM_{2.5} health effects in China during 2000–2011. *Environ. Sci. Pollut. Res. Int.* **2017**, *24*, 10695–10707. [[CrossRef](#)]
2. Donkelaar, A.V.; Martin, R.V.; Brauer, M.; Kahn, R.; Levy, R.; Verduzco, C.; Villeneuve, P.J. Global Estimates of Ambient Fine Particulate Matter Concentrations from Satellite-Based Aerosol Optical Depth: Development and Application. *Environ. Health Perspect.* **2010**, *118*, 847. [[CrossRef](#)] [[PubMed](#)]
3. See, S.W.; Balasubramanian, R. Chemical characteristics of fine particles emitted from different gas cooking methods. *Atmos. Environ.* **2008**, *42*, 8852–8862. [[CrossRef](#)]
4. Pope, R.C.; Dockery, D.W. Health effects of fine particulate air pollution: Lines that connect. *J. Air Waste Manag. Assoc.* **2006**, *56*, 1368–1380. [[CrossRef](#)] [[PubMed](#)]

5. Donkelaar, A.V.; Martin, R.V.; Brauer, M.; Hsu, N.C.; Kahn, R.A.; Levy, R.C.; Lyapustin, A.; Sayer, A.M.; Winker, D.M. Global Estimates of Fine Particulate Matter using a Combined Geophysical-Statistical Method with Information from Satellites, Models, and Monitors. *Environ. Sci. Technol.* **2016**, *50*, 3762. [[CrossRef](#)] [[PubMed](#)]
6. Boys, B.L.; Martin, R.V.; Van, D.A.; Macdonell, R.J.; Hsu, N.C.; Cooper, M.J.; Yantosca, R.M.; Lu, Z.; Streets, D.G.; Zhang, Q. Fifteen-year global time series of satellite-derived fine particulate matter. *Environ. Sci. Technol.* **2014**, *48*, 11109. [[CrossRef](#)] [[PubMed](#)]
7. Hu, X.; Waller, L.A.; Al-Hamdan, M.Z.; Crosson, W.L.; Estes, S.M., Jr.; Quattrochi, D.A.; Sarnat, J.A.; Liu, Y. Estimating ground-level PM (2.5) concentrations in the southeastern U.S. using geographically weighted regression. *Environ. Res.* **2013**, *121*, 1–10. [[CrossRef](#)]
8. Tian, J.; Chen, D. A semi-empirical model for predicting hourly ground-level fine particulate matter (PM 2.5) concentration in southern Ontario from satellite remote sensing and ground-based meteorological measurements. *Remote Sens. Environ.* **2010**, *114*, 221–229. [[CrossRef](#)]
9. Dawson, J.P.; Adams, P.J.; Pandis, S.N. Sensitivity of PM 2.5 to climate in the Eastern U.S.: A modeling case study. *Atmos. Chem. Phys. Discuss.* **2007**, *7*, 4295–4309. [[CrossRef](#)]
10. Hu, X.; Waller, L.A.; Lyapustin, A.; Wang, Y.; Al-Hamdan, M.Z.; Crosson, W.L.; Estes, S.M., Jr.; Quattrochi, D.A.; Puttaswamy, S.J. Estimating ground-level PM 2.5 concentrations in the Southeastern United States using MAIAC AOD retrievals and a two-stage model. *Remote Sens. Environ.* **2014**, *140*, 220–232. [[CrossRef](#)]
11. Engel-Cox, J.A.; Hoff, R.M. Qualitative and quantitative evaluation of MODIS satellite sensor data for regional and urban scale air quality. *Atmos. Environ.* **2004**, *38*, 2495–2509. [[CrossRef](#)]
12. Wang, J.; Christopher, S.A. Intercomparison between satellite-derived aerosol optical thickness and PM 2.5 mass: Implications for air quality studies. *Geophys. Res. Lett.* **2003**, *30*, 267–283. [[CrossRef](#)]
13. Yao, F.; Si, M.; Li, W.; Wu, J. A multidimensional comparison between MODIS and VIIRS AOD in estimating ground-level PM 2.5 concentrations over a heavily polluted region in China. *Sci. Total Environ.* **2018**, *618*, 819–828. [[CrossRef](#)] [[PubMed](#)]
14. Sreekanth, V.; Mahesh, B.; Niranjan, K. Satellite Remote Sensing of Fine Particulate air pollutants over Indian Mega Cities. *Adv. Space Res.* **2017**, *60*, 2268–2276. [[CrossRef](#)]
15. Ma, Z.; Hu, X.; Sayer, A.M.; Levy, R.; Zhang, Q.; Xue, Y.; Tong, S.; Bi, J.; Huang, L.; Liu, Y. Satellite-Based Spatiotemporal Trends in PM 2.5 Concentrations: China, 2004–2013. *Env. Health Perspect.* **2016**, *124*, 184–192. [[CrossRef](#)] [[PubMed](#)]
16. Zhang, Y.; Li, Z. Remote sensing of atmospheric fine particulate matter (PM 2.5) mass concentration near the ground from satellite observation. *Remote Sens. Environ.* **2015**, *160*, 252–262. [[CrossRef](#)]
17. Lee, H.J.; Liu, Y.; Coull, B.A.; Schwartz, J.; Koutrakis, P. A novel calibration approach of MODIS AOD data to predict PM 2.5 concentrations. *Atmos. Chem. Phys.* **2011**, *11*, 9769–9795. [[CrossRef](#)]
18. You, W.; Zang, Z.; Pan, X.; Zhang, L.; Chen, D. Estimating PM 2.5 in Xi'an, China using aerosol optical depth: A comparison between the MODIS and MISR retrieval models. *Sci. Total Environ.* **2015**, *505*, 1156–1165. [[CrossRef](#)]
19. Liu, Y.; Franklin, M.; Kahn, R.; Koutrakis, P. Using aerosol optical thickness to predict ground-level PM 2.5 concentrations in the St. Louis area: A comparison between MISR and MODIS. *Remote Sens. Environ.* **2007**, *107*, 33–44. [[CrossRef](#)]
20. Liu, Y.; Paciorek, C.J.; Koutrakis, P. Estimating regional spatial and temporal variability of PM 2.5 concentrations using satellite data, meteorology, and land use information. *Environ. Health Perspect.* **2009**, *117*, 886. [[CrossRef](#)]
21. Zhang, X.; Hu, H. Improving Satellite-Driven PM 2.5 Models with VIIRS Nighttime Light Data in the Beijing-Tianjin-Hebei Region, China. *Remote Sens.* **2017**, *9*, 908. [[CrossRef](#)]
22. Wang, J.; Aegeuter, C.; Xu, X.; Szykman, J.J. Potential application of VIIRS Day/Night Band for monitoring nighttime surface PM 2.5 air quality from space. *Atmos. Environ.* **2016**, *124*, 55–63. [[CrossRef](#)]
23. Li, W.; Zeng, R.; Wu, J. Remote sensing monitoring of ground-level PM 2.5 concentrations in China: A comparison between VIIRS and MODIS. In Proceedings of the Association of American Geographers (AAG) Annual Meeting 2014, Tampa, FL, USA, 8–12 April 2014.
24. Wang, W.; Mao, F.; Du, L.; Pan, Z.; Gong, W.; Fang, S. Deriving Hourly PM 2.5 Concentrations from Himawari-8 AODs over Beijing-Tianjin-Hebei in China. *Remote Sens.* **2017**, *9*, 858. [[CrossRef](#)]

25. Van, D.A.; Martin, R.V.; Brauer, M.; Boys, B.L. Use of Satellite Observations for Long-Term Exposure Assessment of Global Concentrations of Fine Particulate Matter. *Environ. Health Perspect.* **2015**, *123*, 135.
26. Liu, Y.; Park, R.J.; Jacob, D.J.; Li, Q.; Kilaru, V.; Sarnat, J.A. Mapping annual mean ground-level PM 2.5 concentrations using Multiangle Imaging Spectroradiometer aerosol optical thickness over the contiguous United States. *J. Geophys. Res. Atmos.* **2004**, *109*. [[CrossRef](#)]
27. He, Q.; Zhou, G.; Geng, F.; Gao, W.; Yu, W. Spatial distribution of aerosol hygroscopicity and its effect on PM 2.5 retrieval in East China. *Atmos. Res.* **2016**, *170*, 161–167. [[CrossRef](#)]
28. Lin, C.; Li, Y.; Lau, A.K.H.; Deng, X.; Tse, T.K.T.; Fung, J.C.H.; Li, C.; Li, Z.; Lu, X.; Zhang, X. Estimation of long-term population exposure to PM 2.5 for dense urban areas using 1-km MODIS data. *Remote Sens. Environ.* **2016**, *179*, 13–22. [[CrossRef](#)]
29. Xiao, Q.; Wang, Y.; Chang, H.H.; Meng, X.; Geng, G.; Lyapustin, A.; Liu, Y. Full-coverage high-resolution daily PM 2.5 estimation using MAIAC AOD in the Yangtze River Delta of China. *Remote Sens. Environ.* **2017**, *199*, 437–446. [[CrossRef](#)]
30. Sun, K.; Chen, X. Spatio-temporal distribution of localized aerosol loading in China: A satellite view. *Atmos. Environ.* **2017**, *163*, 35–43. [[CrossRef](#)]
31. Chen, Q.X.; Yuan, Y.; Huang, X.; Jiang, Y.Q.; Tan, H.P. Estimation of surface-level PM 2.5 concentration using aerosol optical thickness through aerosol type analysis method. *Atmos. Environ.* **2017**, *159*, 26–33. [[CrossRef](#)]
32. Lin, C.Q.; Li, Y.; Yuan, Z.B.; Lau, A.K.H.; Li, C.C.; Fung, J.C.H. Using satellite remote sensing data to estimate the high-resolution distribution of ground-level PM 2.5. *Remote Sens. Environ.* **2015**, *156*, 117–128. [[CrossRef](#)]
33. Gao, C.; Zhang, X.L.; Wang, W.Y.; Xiu, A.J.; Tong, D.Q.; Chen, W.W. Spatiotemporal Distribution of satellite-retrieved ground-level PM 2.5 and near real-time daily retrieval algorithm development in Sichuan Basin, China. *Atmosphere* **2018**, *9*, 78. [[CrossRef](#)]
34. Chen, G.B.; Li, S.S.; Knibbs, L.D.; Hamm, N.A.S.; Cao, W.; Li, T.T.; Guo, J.P.; Ren, H.Y.; Abramson, M.J.; Guo, Y.M. A machine learning method to estimate PM 2.5 concentrations across China with remote sensing, meteorological and land use information. *Sci. Total Environ.* **2018**, *636*, 52–60. [[CrossRef](#)] [[PubMed](#)]
35. Wang, Y.S.; Xin, J.Y.; Li, Z.Q.; Wang, P.C.; Wang, S.G.; Wen, T.X.; Sun, Y. AOD and Angstrom parameters of aerosols observed by the Chinese Sun Hazemeter Network from August to December 2004. *Environ. Sci. 2006*, *27*, 1703–1711.
36. Aeronet.gsfc.nasa.gov. Aerosol Robotic Network (AERONET) Homepage. Available online: <https://aeronet.gsfc.nasa.gov> (accessed on 7 March 2020).
37. Bou.class.noaa.gov. NOAA's Comprehensive Large Array-data Stewardship System. Available online: <https://www.bou.class.noaa.gov/saa/products/welcome> (accessed on 7 March 2020).
38. Ouyang, S.H. Summarization on PM 2.5 Online Monitoring Technique. *China Environ. Prot. Ind.* **2012**, *13*, 14–18.
39. Gupta, P.; Christopher, S.A.; Wang, J.; Gehrig, R.; Lee, Y.; Kumar, N. Satellite remote sensing of particulate matter and air quality assessment over global cities. *Atmos. Environ.* **2006**, *40*, 5880–5892. [[CrossRef](#)]
40. Barman, S.C.; Singh, R.; Negi, M.P.S.; Bhargava, S.K. Fine Particles (PM 2.5) in Residential Areas of Lucknow City and Factors Influencing the Concentration. *Clean Soil Air Water* **2010**, *36*, 111–117. [[CrossRef](#)]
41. Pateraki, S.; Asimakopoulos, D.N.; Flocas, H.A.; Maggos, T.; Vasilakos, C. The role of meteorology on different sized aerosol fractions (PM 10, PM 2.5, PM 2.5–10). *Sci. Total Environ.* **2012**, *419*, 124–135. [[CrossRef](#)]
42. Liu, Y.; Sarnat, J.A.; Kilaru, V.; Jacob, D.J.; Koutrakis, P. Estimating ground-level PM 2.5 in the eastern United States using satellite remote sensing. *Environ. Sci. Technol.* **2005**, *39*, 3269. [[CrossRef](#)]
43. ECMWF. ECMWF. Available online: <http://www.ecmwf.int/> (accessed on 7 March 2020).
44. Srtm.cgiar.org. CGIAR-CSI SRTM—SRTM 90m DEM Digital Elevation Database. Available online: <http://srtm.cgiar.org/> (accessed on 7 March 2020).
45. Song, W.; Jia, H.; Huang, J.; Zhang, Y. A satellite-based geographically weighted regression model for regional PM 2.5 estimation over the Pearl River Delta region in China. *Remote Sens. Environ.* **2014**, *154*, 1–7. [[CrossRef](#)]
46. Zeng, Q.; Wang, Z.; Tao, J.; Wang, Y.; Chen, L.; Zhu, H.; Yang, J.; Wang, X.; Li, B. Estimation of Ground-Level PM 2.5 Concentrations in the Major Urban Areas of Chongqing by Using FY-3C/MERSI. *Atmosphere* **2017**, *9*, 3. [[CrossRef](#)]
47. Zhao, S.; Yu, Y.; Yin, D.; Qin, D.; He, J.; Dong, L. Spatial patterns and temporal variations of six criteria air pollutants during 2015 to 2017 in the city clusters of Sichuan Basin, China. *Sci. Total Environ.* **2017**, *624*, 540–557. [[CrossRef](#)] [[PubMed](#)]

48. Zou, J.; Yang, L. The ambient air quality and trends in cities of Sichuan province. *Sichuan Environ.* **2010**, *29*, 4.
49. Xu, J.H.; Jiang, H. Estimation of PM 2.5 concentration over the Yangtze Delta using remote sensing: Analysis of spatial and temporal variations. *Environ. Sci.* **2015**, *36*, 3119–3127.
50. Zeng, Q.; Wang, Y.; Chen, L.; Wang, Z.; Zhu, H.; Li, B. Inter-Comparison and Evaluation of Remote Sensing Precipitation Products over China from 2005 to 2013. *Remote Sens.* **2018**, *10*, 168. [[CrossRef](#)]
51. Chen LW, A.; Chow, J.C.; Doddridge, B.G.; Dickerson, R.R.; Ryan, W.F.; Mueller, P.K. Analysis of a summertime PM 2.5 and haze episode in the mid-Atlantic region. *Air Repair* **2003**, *53*, 946–956.
52. Zhu, S.; Zhou, M.; Qiao, L.; Li, L.; Lou, S.; Yan, S.; Chen, C. Impact of the air mass trajectories on PM 2.5 concentrations and distribution in the Yangtze River Delta in December 2015. *J. Environ. Sci.* **2015**, *36*, 10.
53. Chen, N.; Xu, K.; Cao, Z.; Liu, D.; Hu, H.; Quan, J.; Xinjiang Jinghe County Environmental Protection Bureau. Analysis on the pollution levels of atmospheric particles and the correlation of pollutants in hHubei province. *Environ. Sci. Technol.* **2016**, *39*, 194–198.
54. Deng, X.; Huang, Y.; Li, Z.; Li, H. Temporal and spatial variations characteristics of atmospheric particulate matter in Hubei province, China. *J. Environ. Sci.* **2017**, *11*, 5152–5158.
55. Tian, P.; Cao, X.; Zhang, L.; Sun, N.; Sun, L.; Logan, T.; Huang, Z. Aerosol vertical distribution and optical properties over China from long-term satellite and ground-based remote sensing. *Atmos. Chem. Phys.* **2017**, *17*, 2509–2523. [[CrossRef](#)]
56. Dubovik, O.; Holben, B.; Eck, T.F.; Smirnov, A.; Kaufman, Y.J.; King, M.D.; Tanré, D.; Slutsker, I. Variability of Absorption and Optical Properties of Key Aerosol Types Observed in Worldwide Locations. *J. Atmos. Sci.* **2002**, *59*, 590–608. [[CrossRef](#)]



© 2020 by the authors. Licensee MDPI, Basel, Switzerland. This article is an open access article distributed under the terms and conditions of the Creative Commons Attribution (CC BY) license (<http://creativecommons.org/licenses/by/4.0/>).